

Differential enhancement of ERK, PKA and Ca²⁺ signaling in direct and indirect striatal neurons of Parkinsonian mice



Louise-Laure Mariani^{a,b,c}, Sophie Longueville^{a,b,c}, Jean-Antoine Girault^{a,b,c}, Denis Hervé^{a,b,c,*}, Nicolas Gervasi^{a,b,c,*}

^a Inserm UMR-S 1270, Paris, France

^b Sorbonne Université, Science and Engineering Faculty, Paris, France

^c Institut du Fer à Moulin, Paris, France

ARTICLE INFO

Keywords:

Parkinson's disease
Striatum
Striatal projection neuron
6-hydroxydopamine
Mouse
Ca²⁺ signaling
cAMP signaling
ERK
Biosensors
Förster resonance energy transfer
Two-photon microscopy

ABSTRACT

Parkinson's disease (PD) is characterized by severe locomotor deficits due to the disappearance of dopamine (DA) from the dorsal striatum. The development of PD symptoms and treatment-related complications such as dyskinesia have been proposed to result from complex alterations in intracellular signaling in both direct and indirect pathway striatal projection neurons (dSPNs and iSPNs, respectively) following loss of DA afferents. To identify cell-specific and dynamical modifications of signaling pathways associated with PD, we used a hemiparkinsonian mouse model with 6-hydroxydopamine (6-OHDA) lesion combined with two-photon fluorescence biosensors imaging in adult corticostriatal slices. After DA lesion, extracellular signal-regulated kinase (ERK) activation was increased in response to DA D1 receptor (D1R) or α -amino-3-hydroxy-5-methyl-4-isoxazolepropionic acid (AMPA) stimulation. The cAMP-dependent protein kinase (PKA) pathway contributing to ERK activation displayed supersensitive responses to D1R stimulation after 6-OHDA lesion. This cAMP/PKA supersensitivity was specific of D1R-responding SPNs and resulted from G α_{olf} upregulation and deficient phosphodiesterase activity. In lesioned striatum, the number of D1R-SPNs with spontaneous Ca²⁺ transients augmented while Ca²⁺ response to AMPA receptor stimulation specifically increased in iSPNs. Our work reveals distinct cell type-specific signaling alterations in the striatum after DA denervation. It suggests that over-activation of ERK pathway, observed in PD striatum, known to contribute to dyskinesia, may be linked to the combined dysregulation of DA and glutamate signaling pathways in the two populations of SPNs. These findings bring new insights into the implication of these respective neuronal populations in PD motor symptoms and the occurrence of PD treatment complications.

1. Introduction

The striatum is the main input structure of the basal ganglia, which play a major role in motor control, and habitual and goal-directed actions (Redgrave et al., 2010). The functions of the striatum are based on the balance of two distinct populations of GABAergic striatal projection neurons (SPNs, a.k.a. medium-size spiny neurons). SPN activity is driven by abundant glutamatergic inputs from the cerebral cortex and some thalamic nuclei. The direct pathway SPNs (dSPNs) directly project to the basal ganglia output structures (*substantia nigra pars reticulata* and

globus pallidus pars interna) and promote selected actions. The indirect pathway SPNs (iSPNs), in contrast, project to the same output structures through relays in the *globus pallidus pars externa* and subthalamic nucleus, and suppress unselected actions (Albin et al., 1989). Dopamine (DA) released by afferent neurons from the *substantia nigra pars compacta* positively activates dSPNs and inhibits iSPNs, which preferentially express DA D1 (D1R) and D2 (D2R) receptors, respectively (Gerfen et al., 1990).

In Parkinson's disease (PD), the progressive loss of DA afferents to the dorsal striatum (caudate nucleus and putamen) is responsible for

Abbreviations: 6-OHDA, 6-hydroxydopamine; AAV, adeno-associated virus; ACSF, artificial cerebrospinal fluid; AKAR3, cAMP-dependent protein kinase activity reporter; D1R, dopamine D1 receptor; D2R, dopamine D2 receptor; DA, dopamine; EKAR-EV, ERK activity reporter; ERK, extracellular signal-regulated kinase; FRET, Förster resonance energy transfer; L-DOPA, L-3,4-dihydroxyphenylalanine; PD, Parkinson's disease; PKA, cAMP-dependent protein kinase/protein kinase A; SPN, striatal projection neuron; dSPN, direct pathway SPN; iSPN, indirect pathway SPN; TH, tyrosine hydroxylase; ROI, region of interest; CFP, cyan fluorescent protein; YFP, yellow fluorescent protein.

* Corresponding authors at: Institut du Fer à Moulin, Inserm UMR-S 1270, Team Neurotransmission and Signaling, 17 rue du Fer à Moulin, 75005 Paris, France.

E-mail addresses: denis.herve@inserm.fr (D. Hervé), nicolas.gervasi@inserm.fr (N. Gervasi).

<https://doi.org/10.1016/j.nbd.2019.104506>

Received 5 March 2019; Received in revised form 6 June 2019

Available online 17 June 2019

0969-9961/ © 2019 Elsevier Inc. All rights reserved.

the motor and possibly non-motor symptoms. Bradykinesia, akinesia, and rigidity are attributed to the loss of dSPN activation and iSPN inhibition (Albin et al., 1989; Alcacer et al., 2017; Kravitz et al., 2010). Various alterations of signaling pathways have been reported in PD patients and animal models of DA neuron lesion. Extracellular signal-regulated kinase (ERK) can be activated by the stimulation of corticostriatal afferents in the intact striatum (Gerfen et al., 2002; Sgambato et al., 1998), but following lesion of DA neurons, ERK becomes very strongly activated by DA replacement therapy, L-3,4-dihydroxyphenylalanine (L-DOPA) (Darmopil et al., 2009; Gerfen et al., 2002; Pavón et al., 2006; Santini et al., 2007; Westin et al., 2007) in a cAMP/protein kinase A(PKA)- and Ca^{2+} -dependent manner (Alcacer et al., 2012; Fieblinger et al., 2014a; Santini et al., 2007). The cAMP/PKA pathway is strongly activated in response to D1R stimulation in the DA-denervated striatum (Santini et al., 2007). In the dorsal striatum, cAMP concentration reflects the balance between its production, depending on the levels of $G\alpha_{olf}$ (Hervé, 2011), the G protein subunit which couples D1R to adenylyl cyclase (AC) (Corvol et al., 2001), and its degradation, through phosphodiesterase (PDE) activity (Nishi et al., 2008; Polito et al., 2015). However the dynamics and cell type specificity of signaling alterations in SPNs resulting from the chronic absence of DA are still poorly characterized, hampering our understanding of their pathophysiological consequences.

To identify the alterations of ERK, cAMP, and Ca^{2+} -dependent pathways in dSPNs and iSPNs in a chronic rodent model of PD, we used fluorescent biosensors for two-photon imaging of identified living neurons in mouse corticostriatal slices. We used Förster resonance energy transfer (FRET)-based biosensors, ERK activity reporter (EKAR-EV) and cAMP-dependent protein kinase (PKA) activity reporter (AKAR3) (Allen and Zhang, 2006; Castro et al., 2013; Komatsu et al., 2011) and we monitored Ca^{2+} dynamics with the Ca^{2+} indicator (GCaMP6s) (Chen et al., 2013). Striatal DA terminals were lesioned by local microinjection of 6-hydroxydopamine (6-OHDA). The responses in intact and DA-denervated striatum were compared following application of D1R agonist and/or AMPA, mimicking the effects of dopaminergic and glutamatergic afferents. We found specific increased activity of ERK- and cAMP/PKA-dependent pathways in response to D1R stimulation without modification of Ca^{2+} signaling in response to AMPA. In contrast, in iSPNs, AMPA-induced Ca^{2+} transients were increased in the DA-denervated striatum, while the cAMP-dependent pathways was not significantly affected. Hence our results indicate that DA and glutamate-induced responses were differentially disrupted in dSPNs and iSPNs. They also suggest that complications in the PD treatments at late stages may be linked to the inability to appropriately regularize both DA and glutamate responses in both populations.

2. Materials and methods

2.1. Animals

C57BL/6JRj mice (Janvier Labs; Le Genest Saint Isle, France) were used for experiments in wild type animals, aged P8-P20 for experiments in young animals and aged from 6 to 8 weeks for experiments in adult males. $Gnal^{+/-}$ mice ($Gnal^{tm1Rax}$, (Belluscio et al., 1998)) were mated with C57BL/6J mice (Charles River Lab France; L'Arbresle, France) to produce male and female $Gnal^{+/-}$ and $Gnal^{+/+}$ littermates. Adult $Drd1::Cre$ [Tg(Drd1a-cre)EY262Gsat, (Gong et al., 2007)] and $Adora2a::Cre$ [Tg(Adora2a-cre)2MDkde, (Durieux et al., 2009)] mice in which the Cre recombinase is targeted to specific neuronal subtypes, were backcrossed for at least 10 generations on a C57BL/6J background. The mice were genotyped by PCR analysis of genomic DNA using standard PCR protocols. The mice were kept in groups (maximum five per cage) on a 12h light/dark cycle at a constant temperature of 22 °C with access to food and water ad libitum. All experiments were in accordance with the guidelines of the French Agriculture and Forestry Ministry for handling animals (decree 87-848). The animal facility was

approved licensed by the *Sous-Direction de la Protection Sanitaire et de l'Environnement de la Préfecture de Police (arrêté préfectoral DTPP 2018-20, D 75-05-22)*. The experimental protocols were approved by the *Ministère de l'éducation nationale, de l'enseignement supérieur et de la recherche* (authorization # 02635.02). The principal investigators had a personal agreement (D.H., license C-75-828; J.-A.G., license 75-877).

2.2. 6-OHDA lesions, AAV injections and postoperative care

Mice were anesthetized with a mixture of xylazine (10 mg/kg) and ketamine (75 mg/kg) (Centravet) and mounted in a digitalized stereotaxic frame (Stoelting Europe) equipped with a mouse adaptor. 6-OHDA-HCl (6.0 mg/ml, Sigma-Aldrich) was dissolved in a solution containing 0.2 g/L ascorbic acid in saline. The AAV stock suspension was diluted 5 times in the 6-OHDA ascorbic acid solution. Mice received a unilateral injection (1.25 μ L) of a mix of 6-OHDA and AAV into the right striatum at the following coordinates according to a mouse brain atlas (Paxinos and Franklin, 2001): anteroposterior (AP), +0.3 mm and lateral (L), +2.3 mm from bregma; dorsoventral (DV), -3.4 mm (from the skull surface). Sham mice were injected with vehicle only (ascorbic acid in saline) in which the AAV virus was also diluted 5 times. Before and after surgery, the mice received a subcutaneous injection of a non-steroidal anti-inflammatory drug (flunixin meglumine, 4 mg/kg; Sigma-Aldrich) and were placed on a warm plate during about \approx 10 h after surgery to avoid hypothermia. Mice were allowed to recover for 3 weeks before sacrifice and brain slicing. Lesions were assessed at the end of experiments by determining the striatal levels of tyrosine hydroxylase (TH) using immunoblotting (see below) on the striata from the slice or its adjacent slice. Only animals with a TH level reduction by > 70% in the lesioned striatal area compared with the control side were included in the analyses.

2.3. Biosensors and viral vectors

The GCaMP6s (Chen et al., 2013), FRET-based A-kinase activity reporter AKAR3 (Allen and Zhang, 2006) and ERK activity reporter EKAR-EV (Komatsu et al., 2011) were used in the present study. pAAV.Syn.GCaMP6s.WPRE.SV40 and pAAV.Syn.Flex.GCaMP6s.WPRE.SV40 were a gift from the Genetically Encoded Neuronal Indicator and Effector Project (GENIE) & Douglas Kim (Addgene viral prep # 100843-AAV9 and Addgene viral prep # 100845-AAV1). Plasmids encoding AKAR3 and EKAR-EV were a gift from Jin Zhang and Michiyuki Matsuda respectively. pAAV.hSyn.AKAR3.WPRE was constructed by Ted Abel (University of Pennsylvania) and pAAV.hSyn.EKAREV.WPRE was synthesized from GenScript HK USA and viral preparations were performed by Upenn Vector Core. AAVs were injected into the striatum as described in the corresponding section and brains were typically sliced 2 to 5 weeks after surgery.

2.4. Preparation of brain slices

Before brain removal, the animals were anesthetized with a mixture of xylazine (10 mg/kg) and ketamine (75 mg/kg). Then ice-cold "cutting" choline-artificial cerebrospinal fluid (choline-ACSF) solution, containing (mM) 110 choline Cl, 0.5 $CaCl_2$, 7 $MgCl_2$, 1.25 NaH_2PO_4 , 25 $NaHCO_3$, 2.5 KCl, 11.6 ascorbic acid, 3.1 sodium pyruvate and 25 glucose, saturated with 5% CO_2 and 95% O_2 , was perfused to the brain by intracardiac perfusion. Brains were quickly isolated and placed in ice-cold "cutting" choline-ACSF solution. Sections (250 μ m) were made using a vibrating microtome (Thermo Scientific) in a parahorizontal plane as described previously (Kawaguchi et al., 1989). After cutting, brain slices were transferred 15 min to recover in standard ACSF solution at 35 °C, containing (mM): 125 NaCl, 1 $CaCl_2$, 1 $MgCl_2$, 1.25 NaH_2PO_4 , 26 $NaHCO_3$, 2.5 KCl, and 25 glucose, saturated with 5% CO_2 and 95% O_2 . Brain slices were then kept in a custom-made interface chamber on an optic paper lying on a non-woven compress net, placed

at the interface between the ACSF solution gassed with 95% O₂/5% CO₂ and incubated for 1 h at room temperature in a 95% O₂/5% CO₂ atmosphere, a time needed to recover a pH/metabolic equilibrium.

2.5. Two-photon slice imaging

Experiments were performed at the *Institut du Fer à Moulin* Cell and Tissue Imaging Facility. On the microscope stage, a nylon/platinum harp stabilized the slice while suspended on a nylon mesh to facilitate continuous perfusion over the whole slice at 5 mL/min with ACSF at 32 °C. Two-photon imaging was performed using an upright Leica TCS MP5 microscope with resonant scanning (8 kHz), a Leica 25×/0.95 HCX IRAPO immersion objective and a tunable Ti:sapphire laser (Coherent Chameleon Vision II) with dispersion correction set to 860 nm for CFP excitation (FRET experiments) and 920 nm for GCaMP6s excitation. The emission path consisted of an initial 700 nm low-pass filter to remove excess excitation light (E700 SP, Chroma Technologies), 505 nm dichroic mirror for orthogonal separation of emitted signal, 483/32 CFP emission filter, 535/30 YFP emission filter for AKAR3 and EKAR-EV imaging, and a 560 nm dichroic mirror for orthogonal separation of emitted signal, 525/50 GFP emission filter for GCaMP6s experiments, and a two-channel Leica HyD detector for simultaneous acquisition. Due to the high quantum efficiency and low dark noise of the HyD photodetectors, detector gain was typically set at 10–20% with laser power at 1–5% (which corresponds to a laser power under the objective of 3–5 mW). For AKAR3 and EKAR-EV image acquisition, Z-stack images (12-bit; 512 × 512) were typically acquired every 15 s. The z-step size was 1–2 μm and total stack size was typically 40–60 sections depending on the slice (≈60–120 μm). For GCaMP imaging, z-stack images (12 bits, 512 × 512) were typically acquired every 1 s. The z-step size was 5 μm and total stack size was typically 3 to 5 sections depending on the slice (≈10 to 20 μm).

2.6. Drug treatments

(RS)-AMPA hydrobromide (0.5 μM; Tocris), SKF81297 hydrobromide (10 μM, Tocris), and CGS21680 hydrochloride (10 μM, Biotechne) were freshly prepared in ultrapure Milli-Q water. Forskolin (10 μM; Sigma), U0126 (5 μM, Tocris), and IBMX (10–300 μM; 3-isobutyl-1-methylxanthine or 3,7-dihydro-1-methyl-3-(2-methylpropyl)-1H-purine-2,6-dione; Tocris) were prepared in 100% DMSO. Concentrated stock solutions were diluted in standard ACSF saturated with 95% O₂/5% CO₂ and continuously bubbled during perfusion, final concentration of DMSO 0.1% (vol/vol). The imaging chamber of the microscope was continuously perfused with the recording ACSF solution saturated with 95% O₂/5% CO₂ at a rate of 5 mL/min. For bath application, smoothly switching between different reservoirs allowed for changing the bathing solution to a solution containing drugs, without mechanically disturbing the preparation. For precise time application of the drug, a 18G needle was linked to a Valvebank*4 circuitry (AutoMate Scientific, Inc.) designed for solution-switching use with valve opening at the desired time of compound application with 10 ms accuracy. The pipette holder was mounted onto a micromanipulator, like those used for patch-clamp experiment. The pipette was filled with ACSF or the drug of interest at its final concentration and positioned using the micromanipulator system, in close proximity to the slice.

2.7. Immunoblotting

At the end of the imaging experiments, striata from both sides were separately dissected from each 250-μm-thick corticostriatal slice and were immediately frozen at –80 °C. Striata were sonicated in 10g/L SDS, and placed at 100 °C for 5 min. Aliquots (5 μL) of the homogenate were used for protein determination using a bicinchoninic acid assay kit (Pierce Europe). Equal amounts of total protein (20 μg) were separated

by SDS-PAGE on 4–15% precast gels (Bio-Rad) and transferred electrophoretically to nitrocellulose membranes (GE Healthcare). The membranes were then incubated in TH chicken polyclonal antibodies (AVES, dilution 1:1000), GFP rabbit polyclonal antibodies (Invitrogen, A-6455) and actin monoclonal mouse and rabbit antibodies (Sigma-Aldrich, dilution 1:5000). Secondary antibodies (1:5000) were IRDye 800CW-conjugated anti-chicken IgG; IRDye 800 CW-conjugated anti-mouse IgG, IRDye 700 CW-conjugated anti-mouse IgG and IRDye 700 CW-conjugated anti-rabbit IgG (Rockland Immunochemical). Bound antibodies were visualized using an Odyssey infrared fluorescence detection system (LI-COR), followed by quantification by Odyssey version 1.2 software. Fluorescence intensity values were normalized to actin values for variations in loading and transfer.

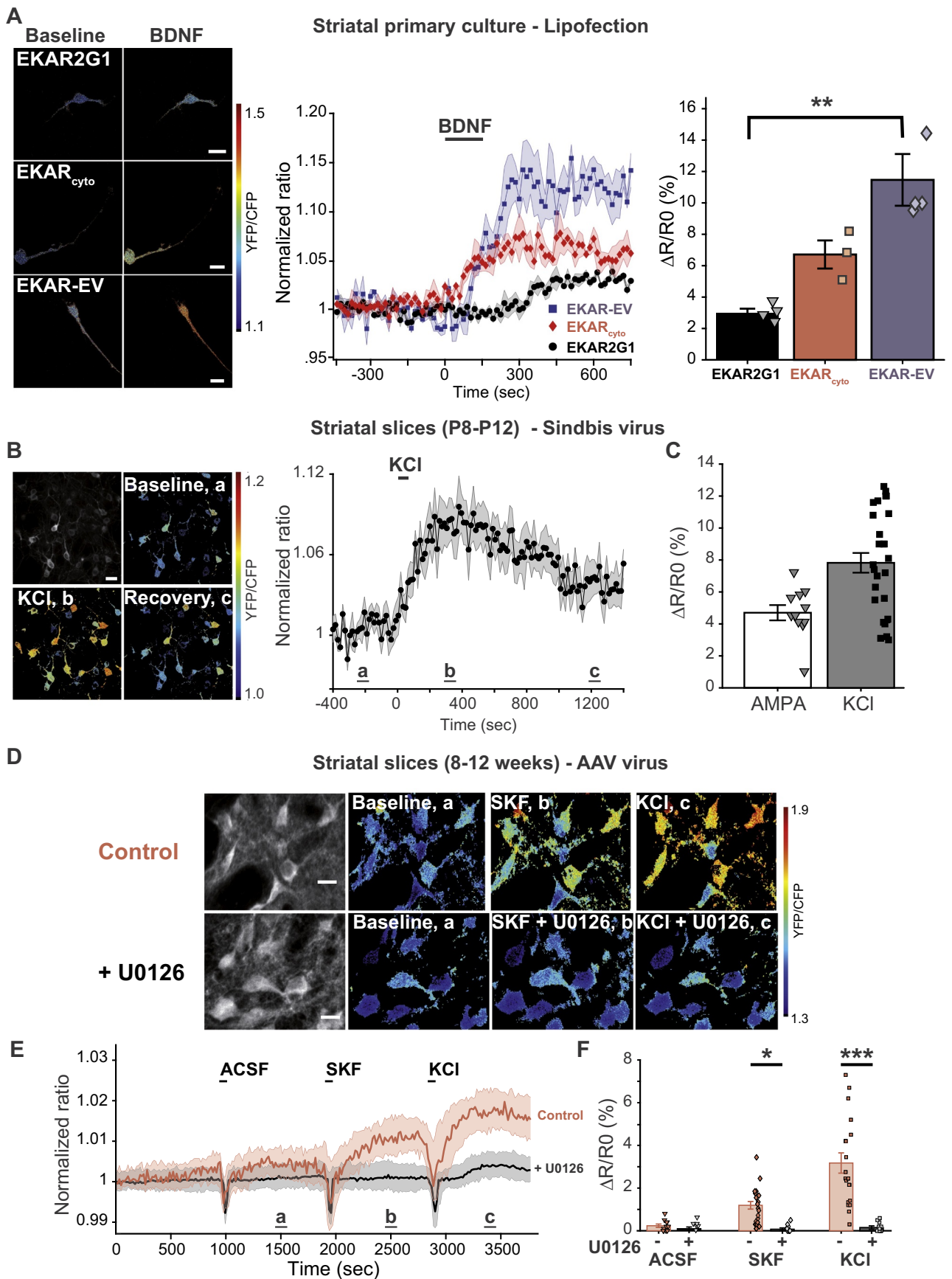
2.8. Image analysis and post-acquisition processing

Images were processed with ImageJ and Icy software by using maximum z projections (ICY-A9L7V2) followed by translation and rotation registration correction to correct for x/y movements and temporal drift (ICY-E4L7S9). Regions of interest (ROIs) were selected for measurement if they could only be measured for the whole experimental time course for AKAR3 and EKAR-EV experiments. For GCaMP experiments, ROI were selected if they appeared during the time course of the experiment, as GCaMP basal fluorescence is usually low and only increases when a response is observed. ROIs were placed around the periphery of the soma. After ROI placement, raw CFP and YFP or GFP intensity measurements for the entire time course were imported into Microsoft Excel (ICY-Y5X4A1). A fluorescence ratio was calculated for each time point in each ROI series and was normalized to the average baseline ratio for each respective ROI (average of 20 to 30 frames during the period before first stimulus) as $\Delta R [YFP/CFP]/R0$ for AKAR3 or EKAR-EV experiments and $\Delta F/F0$ for GCaMP experiments. In all the FRET experiments, responsive cells were defined by two linked parameters: a clear change in the slope of the FRET emission ratio and a change in the amplitude above the baseline noise. In the GCaMP6s experiments, if the amplitude of the fluorescent signal ($\Delta F/F0$) increased over > 3SD (i) during baseline, the cell was considered as “spontaneously active” or (ii) after pharmacological stimulation, the cell was considered as “responsive to treatment” (see Fig. 5A). Statistical analysis was performed in Matlab or GraphPad Prism. Categorical variables are expressed as the percent of the number of responsive cells to a stimulus over the total number of cells assessed; and continuous variables as mean ± SEM. Quantitative variables were compared using a one-way ANOVA followed by Tukey’s multiple comparison test in case of Gaussian distribution or Kruskal-Wallis test followed by Dunn’s multiple comparison test in case of non-Gaussian distribution. Two-tailed, unpaired *t*-test was used to compare quantitative variables when two groups were compared. Categorical variables were compared using the chi-square test or with Fisher exact test when numbers were too small.

3. Results

3.1. Imaging ERK activity dynamics in striatal neurons

In order to monitor ERK activity in striatal neurons we first compared several FRET-based optical biosensors that allow quantitative real-time analysis of ERK activity dynamics with single cell resolution in tissue to determine which one was best suited for our study. We tested EKAR_{cyto}, EKAR2G1, and EKAR-EV (Fritz et al., 2013; Harvey et al., 2008; Komatsu et al., 2011). EKAR_{cyto} is comprised of a fluorescent protein-based FRET pair (mCerulean-mVenus), a phosphorylation substrate peptide containing ERK target sequence (PDVPRTPVGGK) and docking site (FQFP), and the proline-directed WW phospho-binding domain (Harvey et al., 2008). EKAR2G1 uses the backbone of EKAR_{cyto} with a substitution of mCerulean at the N terminus and mVenus at the C



(caption on next page)

Fig. 1. Single-cell spatiotemporal dynamics of ERK activity in SPNs in culture and brain slices.

In all cases, ERK responses were imaged by two-photon microscopy of the indicated FRET biosensor. (A) Comparison of three ERK biosensors in cultured striatal neurons. EKAR_{cyto}, EKAR2G1 or EKAR-EV biosensors were transfected into striatal neurons in culture (DIV 7) using Lipofectamine 2000. Twenty-four hours after lipofection, brain-derived neurotrophic factor (BDNF, 10 ng/mL) was bath-applied for 5 min. Left panel, representative FRET images of ERK biosensors in neurons before (Baseline) and after stimulation with BDNF. All images are pseudo-colored according to the same FRET scale to show the differences in response amplitudes across biosensors. Middle panel, representative time course traces and right panel, maximal amplitude responses ($\Delta R/R_0$ in %) of the indicated ERK biosensors. $**p < 0.01$ for EKAR2G1 versus EKAR-EV (Kruskal–Wallis test followed by Dunn's test, see Table S1). (B) ERK imaging in striatal slice preparations from neonatal mice (P8–P12) using a recombinant Sindbis virus expressing EKAR-EV biosensor. ERK responses were recorded 16–20 h after viral infection. Left panel, two-photon image of YFP channel obtained with a maximal projection of a z stack in the dorsal striatum (top left) and representative FRET images of EKAR-EV before (Baseline, a), 300 s (b) after the beginning of the stimulation with KCl (25 mM, 1 min) and after the recovery (c). Middle panel, representative time course of normalized FRET ratio following 25 mM KCl application (indicated by a horizontal bar) experiment (a, b and c indicate the time at which left panel pictures were taken). (C) Maximal amplitude responses to AMPA (5 μ M, 30 s) and KCl (25 mM, 1 min) responses. (D–E) ERK activation in adult mice striatal slices. Recombinant AAV virus expressing EKAR-EV was stereotactically injected into the striatum 3–5 weeks before imaging. (D) Two-photon image of YFP channel with maximal projection of a z-stack in the dorsal striatum (left pictures) and representative FRET images of EKAR-EV biosensor before (Baseline, a) and after stimulation with SKF81297 (SKF, 10 μ M, b) and KCl (25 mM, c) in ACSF (Control, upper row), or in the presence of a MEK inhibitor (U0126, 5 μ M, lower row). (E) Representative time course of a typical FRET experiment in control condition (red) and with U0126 (black). a, b and c indicate the time at which pictures in D were taken. (F) Maximal amplitudes of FRET ratio responses after application of ACSF (30 s), SKF81297 (10 μ M, 30 s) and KCl (25 mM, 30 s). $*p < 0.05$ for SKF81297 versus SKF81297 + U0126 and $***p < 0.001$ for KCl versus KCl + U0126 (Kruskal–Wallis test followed by Dunn's test, see Table S1). In A, B, and E lines represent the mean value and shaded envelopes indicate SEM. Scale bars, 20 μ m. (For interpretation of the references to colour in this figure legend, the reader is referred to the web version of this article.)

terminus by variants of mTFP1 (mTFP1/cp227) and Venus (Venus/cp173), respectively (Fritz et al., 2013). EKAR-EV is optimized with the YFP/CFP fluorescent protein variant pair (Ypet/ECFP) and a long, flexible linker between the WW domain and the phosphorylation substrate sequence of EKAR_{cyto}, which was shown to markedly increase the gain of FRET signals (Komatsu et al., 2011). To compare their sensitivity, we transfected striatal neurons in culture (DIV 7) with the three EKAR variants using lipofectamine 2000 and we applied on the neurons brain-derived neurotrophic factor (BDNF, 10 ng/mL, for 5 min), which activates ERK signaling through BDNF receptors (Fig. 1A). EKAR-EV exhibited a larger BDNF-induced YFP/CFP emission ratio (FRET ratio) than EKAR_{cyto} and EKAR2G1 (Fig. 1A, middle panel). To quantify FRET responses, we normalized the FRET ratio increases by their corresponding FRET ratio baseline (i.e., $\Delta R/R_0$), as in previous studies (Gervasi et al., 2007, 2010). EKAR-EV showed a higher FRET increase ($12.5 \pm 1.6\%$, mean \pm S.E.M.) than EKAR_{cyto} ($6.6 \pm 0.9\%$) and EKAR2G1 ($2.9 \pm 0.3\%$) (Fig. 1A, right panel). Based on these results, we chose EKAR-EV to monitor ERK activity dynamics in striatal brain slices.

Since Sindbis viruses were previously used to transduce biosensors to monitor other signaling pathways in young brain slices (Castro et al., 2013; Gervasi et al., 2007; Luczak et al., 2017), we used them to express EKAR-EV in striatal slice preparations from immature mice (P8–P12) and monitor changes in ERK activity in real time by ratiometric two-photon microscopy. We first checked whether EKAR-EV was able to report ERK activation in striatal neurons after a global depolarization induced by KCl (25 mM) application for 1 min. This treatment produced, in about 90% of the EKAR-EV-expressing neurons, an increase in the FRET ratio, which peaked around 6 min and then decreased slowly (Fig. 1B middle panel). Application of AMPA (5 μ M) for 30 s or KCl for 1 min yielded an increase in the FRET emission ratio of $4.7 \pm 0.5\%$ and $7.8 \pm 0.6\%$ respectively (mean \pm S.E.M., Fig. 1C).

To study ERK activity dynamics in 6-OHDA-lesioned mice, we needed to perform ERK imaging in mature striatal network (above 8-week old). Since Sindbis virus does not allow effective neuronal infection in adult striatal slices, we produced a recombinant adeno-associated virus (AAV, serotype 2/1) encoding EKAR-EV. The biosensor was expressed in the adult mouse striatum via AAV injection and was subsequently imaged in acute brain slices (2–4 weeks post injection, Fig. 1D). Application of a D1 agonist (SKF81297 10 μ M) for 30 s rapidly increased FRET emission ratio in some of the neuronal somas indicating an increase in ERK activity (Fig. 1E). Subsequent addition of KCl (25 mM) further increased FRET emission ratio ($1.2 \pm 0.2\%$ for SKF81297 versus $3.4 \pm 0.25\%$ for KCl, Fig. 1F). The response to KCl

application was used as a positive control for cell health and responsiveness in all experiments. The SKF81297- and KCl-induced increases in FRET emission ratio were dependent on the activity of mitogen-activated protein kinase/ERK kinases, MEK1/2, the kinases activating ERK, since all the responses were abolished in the presence of U0126 (5 μ M), a selective inhibitor of MEK1/2 (Fig. 1D–F). We noticed that each local application, whatever the drug applied, was followed by a transient decrease in the FRET emission ratio. This decrease also occurred after local application of ACSF whereas ACSF did not produce any significant increase in the FRET emission ratio ($0.15 \pm 0.09\%$). Similar decreases were also recorded in the presence of U0126 for all the stimulations (Fig. 1E). We concluded that these transient decreases in FRET ratio were artefactual and since they were short-lived, they did not preclude measurement of ERK activity after their disappearance. In summary, we showed that EKAR-EV biosensor was appropriate to monitor ERK activity in neurons in culture as well as in young and adult striatal slices.

3.2. Biosensor expression and dopamine depletion after 6-OHDA injection into the striatum of adult mice

We co-injected 6-OHDA and AAV expressing biosensors into the dorsal striatum of 4–6-week old mice that were allowed to recover for 4 weeks before acute brain slicing and two-photon imaging (Fig. 2A). Striatal depletion of DA terminals following 6-OHDA microinjection was checked by the decrease of TH immunoreactivity only in the 6-OHDA-injected side, as indicated by immunoblotting (Fig. 2B). Microinjection of 6-OHDA and DA denervation did not alter the expression of AKAR3 biosensors (Fig. 2C). Similar results were observed when we co-injected 6-OHDA and AAVs expressing EKAR-EV or GCaMP6s biosensors (Fig. 2 C).

3.3. ERK responses are increased after dopamine depletion induced by 6-OHDA lesion

ERK signaling has been reported to be activated by combination of DA D1 and glutamate signals in SPNs in response to drugs of abuse (see (Girault et al., 2007) for a review). Since the activation of ERK is particularly intense after the first L-DOPA treatment in the DA-denervated striatum (Darmopil et al., 2009; Pavón et al., 2006; Santini et al., 2007), we sought to determine whether responsiveness to glutamate or DA or both was increased following the lesion. We compared ERK activity dynamics in response to the application of a DA D1 agonist and/or AMPA stimulation for 30 s, in control and 6-OHDA-lesioned striata. In

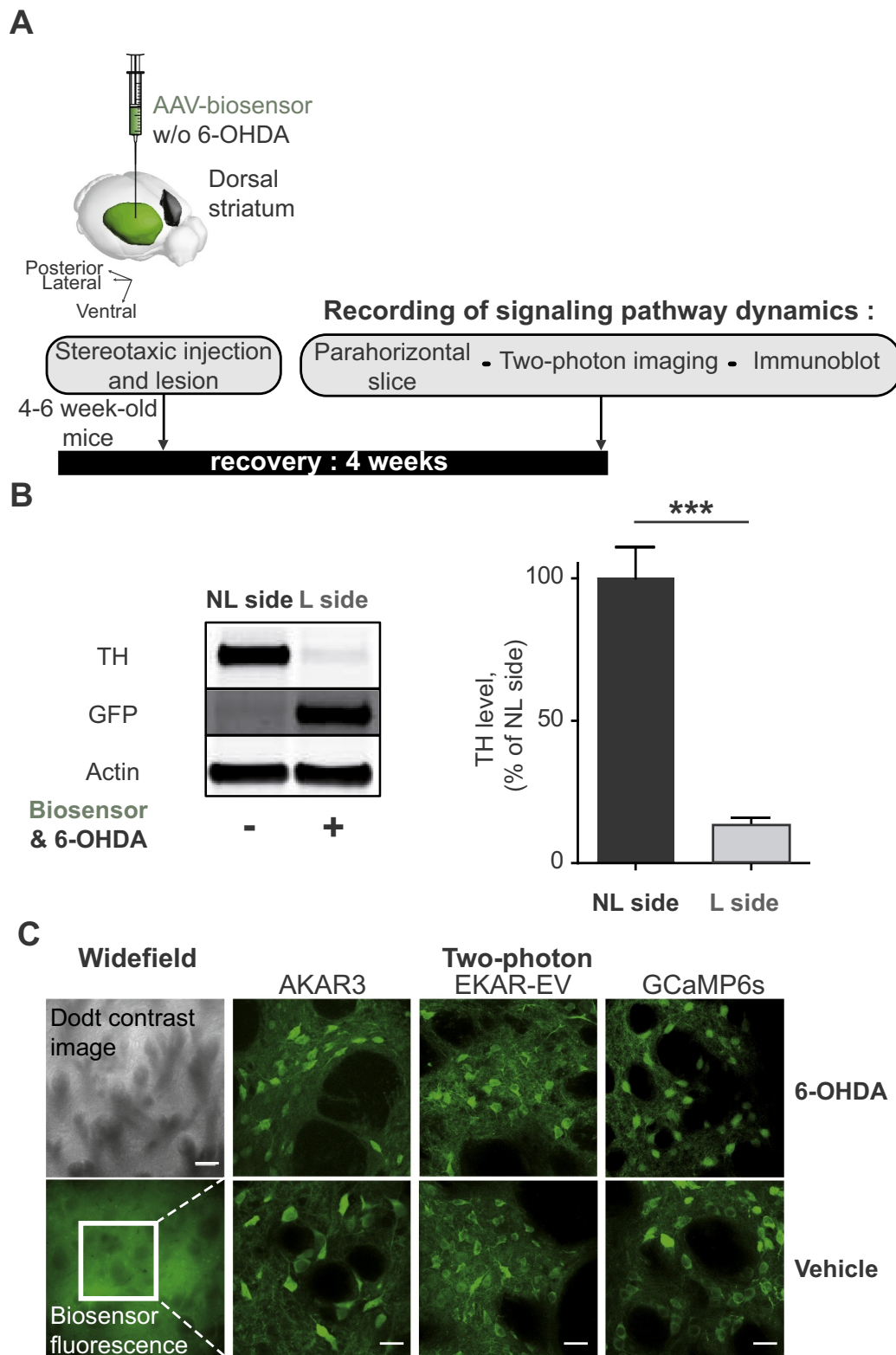


Fig. 2. Biosensor and tyrosine hydroxylase expression after DA-denervation in the dorsal striatum. (A) General experimental design. Mice (4–6-week-old) were injected with a solution containing the biosensor-expressing AAV with or without 6-OHDA in the right striatum. After a 4-week recovery, 2-photon imaging was performed on acute parahorizontal corticostriatal slices. At the end of each experiment, striata were homogenized for TH quantification by immunoblot. (B) Example of immunoblot and quantification of TH levels by immunoblotting. Data are expressed as percentage of the mean in non-lesioned (NL) side and are means \pm SEM. *** $p < 0.001$ for NL versus L side (paired t -test, see Table S1). (C) Stereotaxic co-injection with 6-OHDA of AAV viruses encoding biosensors did not modify biosensor expression. Wide field image of the dorsal striatum in DotD gradient contrast mode (upper left panel) and in the YFP channel (lower left panel). Scale bar 100 μ m. Two-photon images of the dorsal striatum in the YFP excitation/emission channel in mice injected with AAV-AKAR3, EKAR-EV and GCaMP6s with and without 6-OHDA. Scale bar 20 μ m.

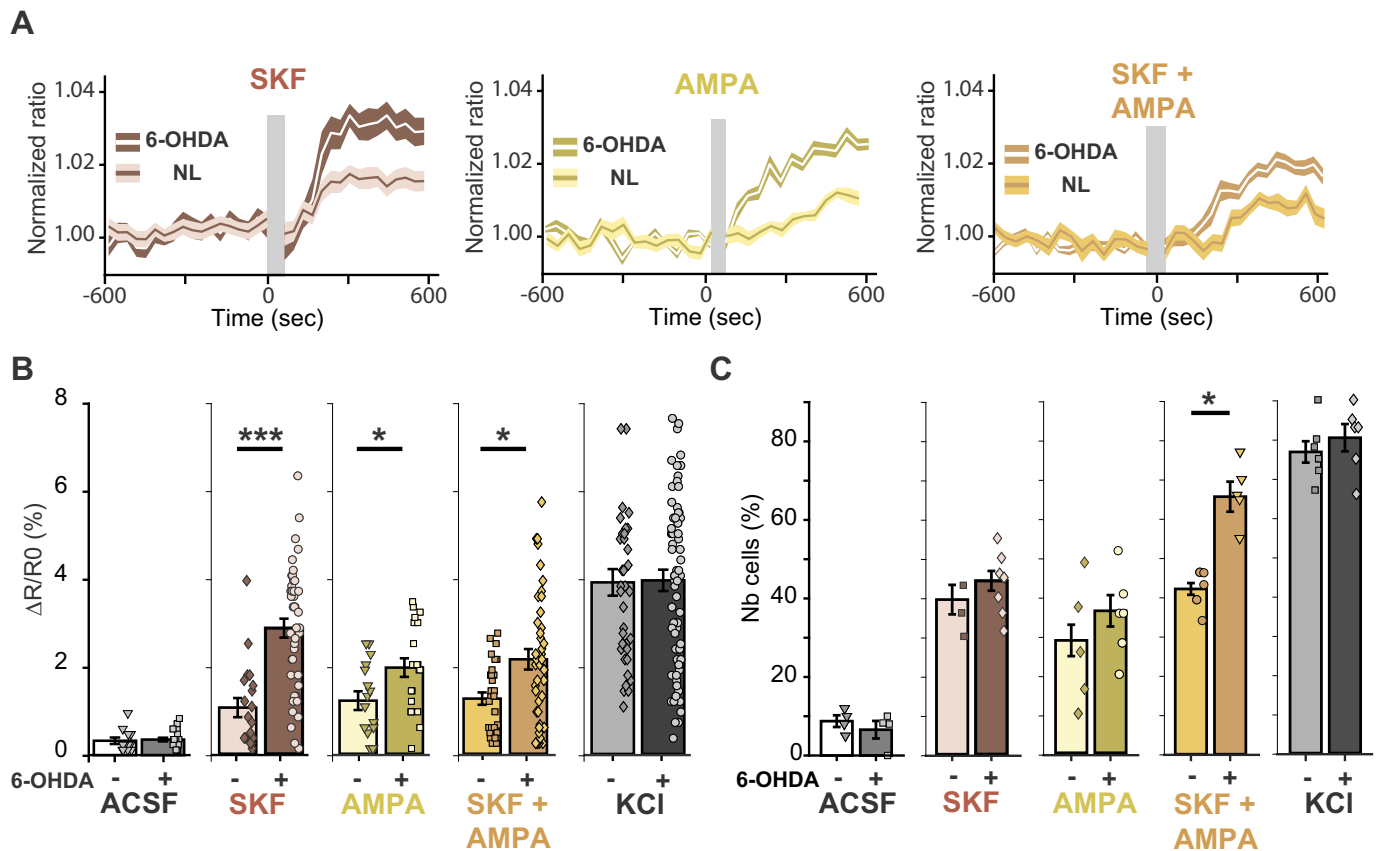


Fig. 3. ERK activity induced by a D1 agonist and AMPA is increased after 6-OHDA lesion in the striatum.

(A) Time course of responses to SKF81297 (SKF, 10 μ M, 30 s), AMPA (2.5 μ M, 30 s) and SKF + AMPA (30 s) in non-lesioned and 6-OHDA lesioned striatum. Gray bars represent the drug application time. The non-specific FRET ratio responses during drug application were removed for a better visualization of normalized ratio changes. (B) ERK maximal amplitude response after application of ACSF (30 s), SKF (10 μ M, 30 s), AMPA (2.5 μ M, 30 s) and KCl (25 mM, 30 s) in 6-OHDA-lesioned (+) and non-lesioned (-) corticostriatal slices (drugs were applied on different slices except for KCl that was added at the end of all the experiments). Mann-Whitney test, see Table S1. (C) Percentage of responsive cells among the total number of EKAR-EV-expressing cells, after the indicated treatments as in B, in 6-OHDA-lesioned (+) and control (-) striatal slices. Mann-Whitney test, see Table S1. * $p < 0.05$, *** $p < 0.001$.

6-OHDA-lesioned striata, this maximal increase after D1R stimulation by SKF81297 (10 μ M) was significantly enhanced as compared to non-lesioned control animals (mean \pm SEM: non-lesioned, $0.9 \pm 0.19\%$, lesioned, $2.4 \pm 0.18\%$, $p < 0.0001$, Fig. 3A and B). AMPA (0.5 μ M) application also produced a higher increase in FRET emission ratio in the 6-OHDA-lesioned striata than in the non-lesioned striata (mean \pm SEM: non-lesioned, $1.0 \pm 0.17\%$, lesioned, $1.6 \pm 0.17\%$, $p < 0.05$, Fig. 3A and B). The co-application of AMPA and SKF81297 increased the FRET emission ratio more in 6-OHDA-lesioned striata than in control striata (non-lesioned, $1.0 \pm 0.12\%$, lesioned, $1.8 \pm 0.19\%$, $p < 0.05$, Fig. 3A and B), although the amplitude of the effects was not increased as compared to those of SKF or AMPA alone. In contrast, the 6-OHDA lesion did not modify the FRET emission ratio of striatal neurons in response to ACSF or KCl (Fig. 3B). We also compared the percentage of neurons responsive to these various stimuli among all the EKAR-EV-expressing neurons in the field of view. In all the FRET experiments, responsive cells were defined by a clear change in the slope of the FRET emission ratio and an increase in the amplitude above the baseline noise. In 6-OHDA-lesioned slices, the percentage of responsive neurons was significantly increased as compared to non-lesioned controls, only after AMPA and SKF81297 co-application (non-lesioned, $43 \pm 3\%$, lesioned, $67 \pm 4\%$, $p < 0.05$, Fig. 3C). The proportion of responsive cells after ACSF, SKF81297, AMPA or KCl application was not modified by the lesion (Fig. 3C).

These results showed upregulation of ERK signaling in response to D1R agonist and/or AMPA after DA denervation by 6-OHDA. The

upregulation of ERK resulted in an increased response amplitude but did not lead to the recruitment of additional cells following stimulation of AMPA receptor or D1R alone. The percentage of responsive neurons to the combined stimulation of D1R and AMPA receptor was increased and reached about 70% of striatal neurons, indicating that ERK was activated in these conditions in both populations of SPNs. The effects of SKF81297 and AMPA on ERK activation in different SPN populations could explain why the co-application of these drugs had no synergistic effect on the amplitude of ERK activation in SPNs. However it appeared that the co-application of SKF81297 and AMPA was able to recruit additional cells. To address the possible mechanisms of the effects of the DA lesion on ERK signaling, we further investigated, the dynamic changes in two signaling pathways leading to ERK activation in SPN, namely the cAMP/PKA pathway, which is activated after D1R stimulation, and the glutamate-induced Ca^{2+} increase.

3.4. PKA responses to D1R stimulation are increased in dSPNs after 6-OHDA lesions

Since an increase in PKA signaling could explain the enhancement of ERK responsiveness to D1R agonist, we investigated PKA responses in control and 6-OHDA-lesioned animals. We injected an AAV vector encoding AKAR3, a biosensor for PKA activity (Allen and Zhang, 2006), into the striatum of adult mice and used corticostriatal slices 3–4 weeks later for real-time imaging of PKA activity (Fig. 4). Since previous studies from other laboratories used very young animals, we first

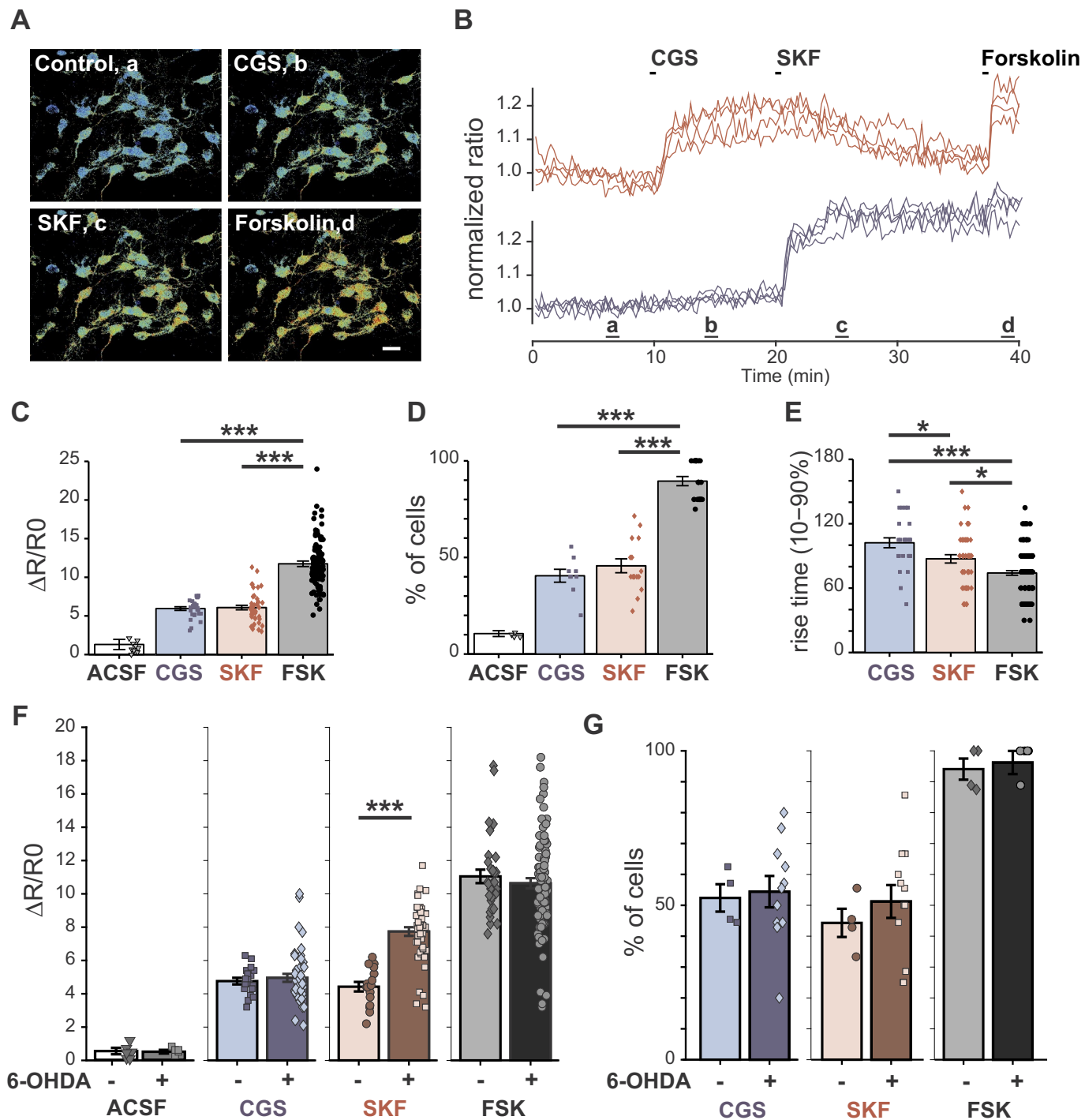


Fig. 4. PKA responses to D1R stimulation are increased in dSPNs after 6-OHDA lesion in the striatum.

(A–B) Identification of putative dSPNs and iSPNs in the dorsal striatum using AKAR3 PKA biosensor 2-photon imaging. (A) Representative FRET pseudocolor images of AKAR3 before (Baseline, a) and after stimulation with an A_{2A} agonist, CGS21680 (CGS, 10 μ M, b), then a D1 agonist, SKF81297 (SKF, 10 μ M, c) and forskolin (FSK, 10 μ M, d). Scale bar, 20 μ m. (B) Time course of a typical AKAR3 experiment. After recording a FRET baseline, sequential application of CGS and SKF was used to activate PKA signaling. Based on their agonist selective responses, neurons were classified as A_{2A} R-expressing SPNs (red) and D1R-expressing SPNs (blue). At the end of the experiment FSK was applied to directly activate AC in both types of neurons. a, b, c and d indicate the time at which pictures in A were taken. Traces for cells responsive to CGS or SKF were separated with different y axes, but they correspond to neurons in the same field and the time axis is the same. (C) AKAR3 maximal responses after application of ACSF, CGS21680 (10 μ M), SKF81297 (10 μ M), and FSK (10 μ M). The order of SKF and CGS application was alternated between slices. Only neurons in which the AKAR3 response to the specific drug or FSK was significant were considered. Kruskal–Wallis followed by Dunn's test, see Table S1. (D) Percentage of responsive cells after treatments as in B. Kruskal–Wallis followed by Dunn's test, see Table S1. (E) Rise time (10–90%) of the same treatments as in B. Kruskal–Wallis followed by Dunn's test, see Table S1. (F–G) Comparison of AKAR3 responses between non-lesioned and 6-OHDA-lesioned striatal slices. (F) Maximal FRET emission ratio responses after application of ACSF, CGS21680 (10 μ M), SKF81297 (10 μ M), and FSK (10 μ M) in non-lesioned mice (–, light colour) and 6-OHDA-lesioned slices (+, dark colour). Mann–Whitney test, see Table S1. (G) Percentage of responsive cells among the total number of AKAR3-expressing cells. Same conditions as in F. (C–G) Error bars indicate SEM, statistical significance of pairwise comparisons, * $p < 0.05$, *** $p < 0.001$. (For interpretation of the references to colour in this figure legend, the reader is referred to the web version of this article.)

validated our approach in adult mice (8–10-week old). As in those previous studies, we stimulated the slices with D1R and A2AR agonists to differentiate putative dSPNs and iSPNs, expected to respond to D1R and A2AR agonists, respectively (Castro et al., 2013; Polito et al., 2015; Yapo et al., 2017). In the dorsal striatum, application of the A2AR agonist CGS21680 (10 μ M) for 1 min yielded an increase in the FRET emission ratio to $5.9 \pm 0.2\%$ (Fig. 4A–C) in less than half of the neurons present in the field of view ($40 \pm 3\%$, Fig. 4D), revealing the A2AR-expressing neurons. After 10 min of CGS21680 washout, application of the D1R agonist, SKF81297 (10 μ M), for 1 min increased FRET emission ratio to $6.1 \pm 0.3\%$ in about the other half of the neurons present in the field of view ($46 \pm 4\%$) (Fig. 4A–D), revealing the D1R-expressing SPN. This was consistent with studies showing that D1R and A2AR are segregated in the two major subsets of SPNs present in equal proportions and globally corresponding to the direct and indirect pathways, respectively (Bertran-Gonzalez et al., 2008; Schiffmann and Vanderhaeghen, 1993). These results were also in agreement with FRET biosensor studies performed in striatal slices from immature mice (Polito et al., 2015; Yapo et al., 2017). We randomly alternated the order of SKF81297 and CGS21680 applications with no effect on either the amplitude of FRET emission ratio or the proportion of responsive SPNs. In all the experiments, a subsequent application of forskolin (FSK, 10 μ M) that directly activates AC, produced a maximal increase in FRET emission ratio to $11.7 \pm 0.3\%$ (Fig. 4A–D), indicating the cell health and the correct AKAR3 responsiveness to AC activation in all experiments. We also measured the rise time of AKAR3 responses that was shorter for FSK than for SKF81297 and longer for CGS21680 (Fig. 4E).

Since these experiments showed that our experimental approach reliably allowed studying PKA responses in adult striatal slices, we then compared PKA activation in control and 6-OHDA-lesioned striata. We co-injected 6-OHDA with an AAV expressing AKAR3 in the dorsal striatum of 4–6-week old mice. In 6-OHDA-lesioned striata, the increase in FRET emission ratio after the application of SKF81297 was significantly higher than in non-lesioned striata (non-lesioned, $4.4 \pm 0.3\%$, lesioned, $7.7 \pm 0.3\%$, $p < 0.001$, Fig. 4F). In contrast, no significant change was detected after application of CGS21680 (non-lesioned, $4.7 \pm 0.2\%$, lesioned, $4.9 \pm 0.3\%$) nor after application of FSK (non-lesioned, $11 \pm 0.5\%$, lesioned, $10.6 \pm 0.4\%$, Fig. 4F). There was no significant change in the percentage of cells responsive to the D1R agonist after 6-OHDA lesion (non-lesioned, $44 \pm 5\%$, lesioned, $50 \pm 5\%$, Fig. 4G). The lesion did not alter either the percentage of cells responsive to the A2AR agonist (non-lesioned, $52 \pm 4\%$, lesioned, $54 \pm 5\%$) or FSK (non-lesioned $94 \pm 3\%$, lesioned, $98 \pm 2\%$, Fig. 4G). Together, these results show that PKA responses are specifically amplified in D1R-expressing SPNs after DA denervation by 6-OHDA lesion, with no change in the number of responsive cells. We then investigated the possible mechanism of this amplification.

3.5. $G\alpha_{olf}$ protein contributes to cell type-specific 6-OHDA-induced increase in PKA activation

In the dorsal striatum, D1R activates AC through its coupling to $G\alpha_{olf}$ (Corvol et al., 2001; Hervé et al., 1993). Increase of $G\alpha_{olf}$ protein levels in the dorsal striatum has been reported after 6-OHDA-lesion (Alcacer et al., 2012; Hervé et al., 1993; Ruiz-DeDiego et al., 2015) and in the putamen of PD patients (Corvol et al., 2004). Therefore, we used $G\alpha_{olf}$ gene (*Gnal*) knockout mice to investigate the mechanism of increased PKA activity after 6-OHDA lesion. Homozygous $G\alpha_{olf}$ gene knockout mice (*Gnal*^{-/-}) have a severe phenotype combining olfactory and striatal deficits (Belluscio et al., 1998; Corvol et al., 2001; Zhuang et al., 2000). These mice usually die in the early postnatal period and could not be used in our study. In contrast, *Gnal*^{+/-} mice, which develop and breed normally, provide an interesting model because they display a decrease of about 50% in $G\alpha_{olf}$ protein levels (Alcacer et al., 2012; Corvol et al., 2007).

We co-injected saline or 6-OHDA with AAV expressing AKAR3 into

the striatum of 4–6 week-old *Gnal*^{+/-} and *Gnal*^{+/+} littermates. When DA innervation was intact, the FRET emission ratio in response to CGS21680 (*Gnal*^{+/+}, $5.2 \pm 0.2\%$, *Gnal*^{+/-}, $3.6 \pm 0.2\%$, $p < 0.001$, Fig. 5A) and SKF81297 application (*Gnal*^{+/+}, $5.9 \pm 0.2\%$, *Gnal*^{+/-}, $3.6 \pm 0.3\%$, $p < 0.001$, Fig. 5B) was lower in *Gnal*^{+/-} mice than in wild type littermates. No change was detected after application of FSK (*Gnal*^{+/+}, $11.4 \pm 0.3\%$, *Gnal*^{+/-}, $11.5 \pm 0.2\%$) meaning that AC was not altered and could still be directly activated by FSK in the *Gnal*^{+/-} mice (Fig. 5C). No significant change was observed in the percentage of responsive cells in *Gnal*^{+/-} mice after CGS21680 (*Gnal*^{+/+}, $36 \pm 3\%$, *Gnal*^{+/-}, $39 \pm 2\%$), SKF81297 (*Gnal*^{+/+}, $50 \pm 3\%$, *Gnal*^{+/-}, $48 \pm 2\%$), or FSK (*Gnal*^{+/+}, $91 \pm 1\%$, *Gnal*^{+/-}, $92 \pm 2\%$). Our results show that the activation of AC by D1R or A2AR is markedly impaired when $G\alpha_{olf}$ protein is reduced, leading to a decreased PKA activation in both populations of SPNs. Our results are in contrast to a study in young mice (P8–12) that do not show any change in PKA responses in *Gnal*^{+/-} mice (Castro et al., 2013). This is likely due to the fact that the $G\alpha_s/G\alpha_{olf}$ switch has not yet fully taken place at P8–12 (Iwamoto et al., 2004) and that AC responses to D1R or A2AR agonists in young mice are less dependent on $G\alpha_{olf}$ levels.

In 6-OHDA-lesioned *Gnal*^{+/-} mice no modification of the FRET emission ratio was observed when CGS21680 was applied when compared to non-lesioned *Gnal*^{+/-} mice (non-lesioned, $3.7 \pm 0.2\%$, lesioned, $3.6 \pm 0.3\%$, Fig. 5A). In contrast, SKF81297 increased the FRET emission ratio to a higher level in 6-OHDA-lesioned *Gnal*^{+/-} mice than in non-lesioned mutant mice (non-lesioned, $3.6 \pm 0.2\%$, lesioned, $6.1 \pm 0.5\%$, $p < 0.001$, Fig. 5B). However, this increase in FRET response did not reach the level attained in 6-OHDA-lesioned striata from wild type mice ($7.8 \pm 0.3\%$ in 6-OHDA-lesioned wild type striata, indicated by a green dashed line in Fig. 5B). No significant change was observed in the FRET emission ratio after FSK application (non-lesioned, $11.1 \pm 0.3\%$, lesioned, $11.9 \pm 0.5\%$, Fig. 5C). In addition, the percentage of responsive cells was unaffected by the lesion in *Gnal*^{+/-} mice after CGS21680 (non-lesioned, $39 \pm 2\%$, lesioned, $42 \pm 2\%$), SKF81297 (non-lesioned, $48 \pm 2\%$, lesioned, $45 \pm 2\%$), or FSK (non-lesioned, $92 \pm 1\%$, lesioned, $89 \pm 2\%$).

These results suggest that in 6-OHDA-lesioned animals, increased PKA activity after D1R stimulation is compatible with an increase in $G\alpha_{olf}$ levels in D1R-expressing SPNs. This increase is cell type-specific because no modification was observed in A2AR-expressing SPNs.

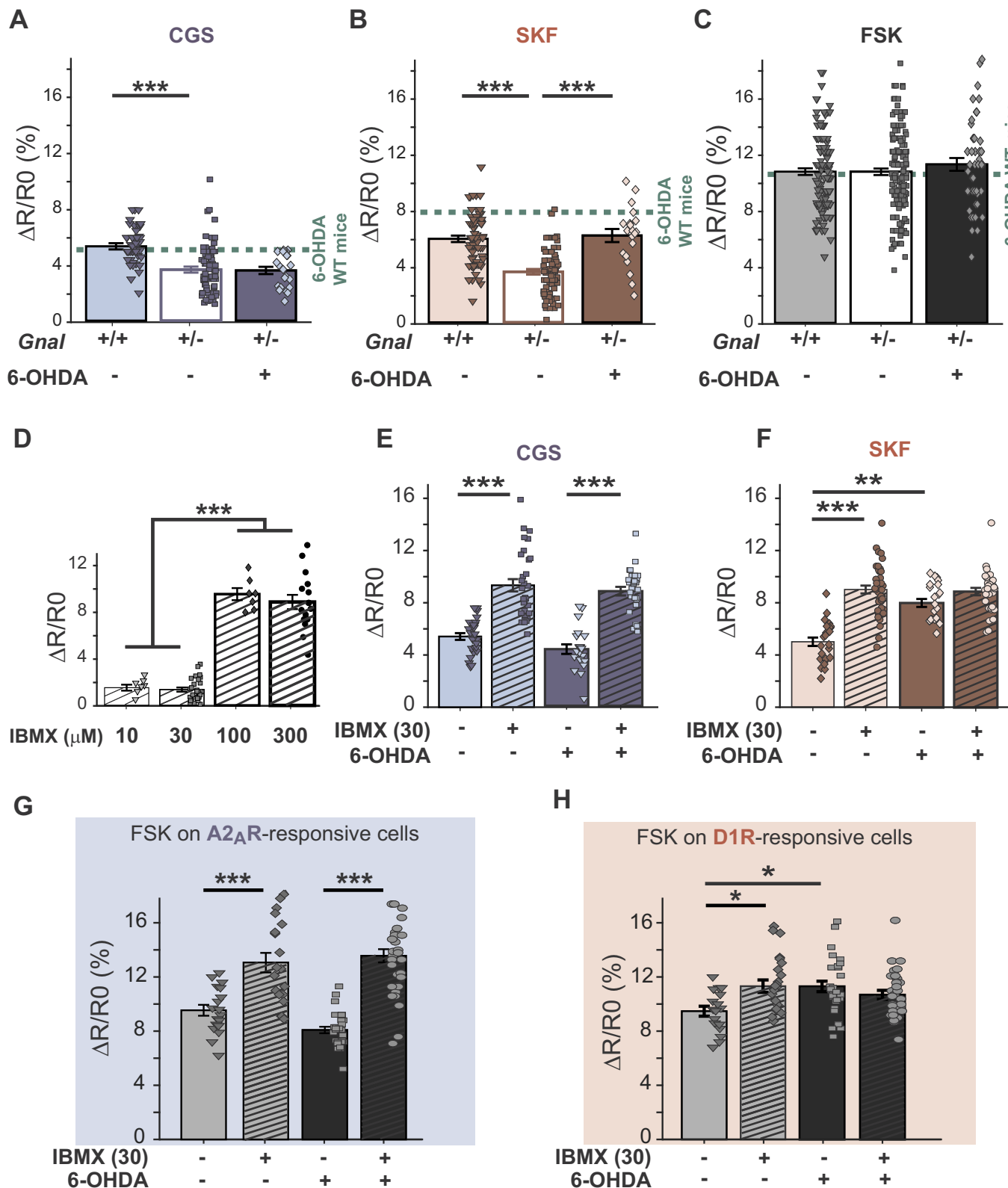
3.6. Cell type-specific decrease in PDE activity contributes to DA lesion-induced increase in PKA

PDEs are important negative regulators of PKA activity. Regulation of the striatal expression of PDEs has been reported in PD patients and animal models of PD, particularly a down-regulation of PDE4 and PDE10 (Heckman et al., 2018; Niccolini et al., 2015, 2017). Hence, up-regulation of PDE activity could be implicated in the cell type-specific up-regulation of PKA activity observed after DA denervation. We examined the effects of application of a broad-spectrum PDE inhibitor, 3-isobutyl-1-methylxanthine (IBMX). We first observed that, as expected, AKAR3 was activated by IBMX in SPNs of adult non-lesioned mice in a dose dependent-manner (Fig. 5D). These results were similar to those previously reported in immature mice (Polito et al., 2015). They showed that in our conditions, cAMP was tonically produced in striatal slices and that PDEs constantly degraded it.

We then investigated PKA responses in adult striatal slices in the presence of a low concentration of IBMX (30 μ M for 10 min), which had no effects on basal FRET emission ratio (Fig. 5D). At this concentration, IBMX enhanced the PKA responses to CGS21680 (no IBMX, $5.4 \pm 0.3\%$, IBMX $9.3 \pm 0.5\%$, $p < 0.001$, Fig. 5E) and SKF81297 (no IBMX, $5.0 \pm 0.3\%$, IBMX $9.0 \pm 0.3\%$, $p < 0.001$, Fig. 5F). This confirmed that PDE activity exerted a strong negative tuning on PKA responses in adult SPNs. In 6-OHDA-lesioned animals, IBMX (30 μ M) also increased the amplitude of FRET emission ratio in response to

CGS21680 (no IBMX, $4.1 \pm 0.3\%$, IBMX, $8.2 \pm 0.3\%$, $p < 0.001$, Fig. 5E). In contrast, it did not further increase the response to SKF81297 (no IBMX, $7.5 \pm 0.3\%$, IBMX $8.2 \pm 0.5\%$, Fig. 5F). Pre-treatment with IBMX did not alter the proportion of responsive cells to the D1R agonist in the 6-OHDA-lesioned striata as compared to non-

lesioned ones (non-lesioned, no IBMX, $39 \pm 7\%$, IBMX, $53 \pm 4\%$; lesioned, no IBMX, $48 \pm 6\%$, IBMX, $54 \pm 5\%$) or A2AR agonist-responsive SPNs (non-lesioned, no IBMX, $44 \pm 7\%$, IBMX, $49 \pm 9\%$, lesioned, no IBMX, $49 \pm 3\%$, IBMX, $48 \pm 4\%$). Our data show a loss of responsiveness of PKA activity to a PDE inhibitor in D1R agonist-



(caption on next page)

Fig. 5. Role of $G\alpha_{\text{olif}}$ and PDEs in the upregulation of PKA response to D1R agonist in the 6-OHDA-lesioned striatum.

(A–C) AKAR3 responses in $A2_A$ R-agonist- and D1R-agonist responsive SPNs in *Gnal* heterozygous mice. (A) Maximal AKAR3 FRET emission ratio in response to CGS21680 (CGS, 10 μ M) in *Gnal*^{+/-} heterozygous mice (expressing 50% of the normal $G\alpha_{\text{olif}}$ levels) without (–) or with (+) 6-OHDA lesion and non-lesioned wild type littermates (*Gnal*^{+/+}) (as in Fig. 4F). For comparison, FRET emission ratio response observed in the 6-OHDA-lesioned striatum of wild type animals (data from Fig. 3F) are indicated by a green dashed line. One-way ANOVA followed by Tukey's test (see Table S1). (B) Same as in A, but in response to SKF81297 (SKF, 10 μ M). (C) Same as in A but in response to forskolin (FSK, 10 μ M). (D–H) Effects of a phosphodiesterase (PDE) inhibitor on AKAR3 responses. (D) Maximal AKAR3 FRET emission ratio in response to the indicated concentrations of the broad-spectrum PDE inhibitor, 3-isobutyl-1-methylxanthine (IBMX), in non-lesioned striatum of wild type mice. Kruskal–Wallis test followed by Dunn's test, see Table S1. (E) Effects of a low concentration of IBMX (30 μ M) on maximal FRET emission ratio responses to CGS21680 (CGS, 10 μ M) in non-lesioned and 6-OHDA-lesioned striatal slices. Kruskal–Wallis test followed by Dunn's test, see Table S1. (F) Same as in E but in response to SKF81297 (SKF, 10 μ M). Kruskal–Wallis test followed by Dunn's test, see Table S1. (G) Effects of 30 μ M IBMX on FSK-induced responses in CGS-responsive cells. One-way ANOVA followed by Tukey's test, see Table S1. (H) Effects of 30 μ M IBMX on FSK-induced responses in SKF-responsive cells. One-way ANOVA followed by Tukey's test, see Table S1. (A–H) Post-hoc pairwise comparisons * $p < 0.05$, *** $p < 0.001$. (For interpretation of the references to colour in this figure legend, the reader is referred to the web version of this article.)

responsive SPNs after 6-OHDA lesion, but not in $A2_A$ R-responsive SPN. Even if the global response to FSK was apparently not changed in lesioned SPNs (see Fig. 4F), we analyzed separately FSK-induced PKA activity in the two types of SPNs to test whether the loss of responsiveness to IBMX was restricted to the D1R pathway or was more generalized in D1R-expressing- SPNs. Pretreatment with IBMX, increased the responses to FSK in the $A2_A$ R agonist-responsive SPNs in non-lesioned (no IBMX, $8.9 \pm 0.4\%$, IBMX, $12.4 \pm 0.8\%$, $p < 0.001$) and 6-OHDA-lesioned slices (no IBMX, $8.2 \pm 0.4\%$, IBMX, $13.7 \pm 0.5\%$, $p < 0.001$, Fig. 5G). The pretreatment with IBMX also increased the responses to FSK in the D1R-expressing SPNs of non-lesioned slices (no IBMX, $9.6 \pm 0.5\%$, IBMX, $11.3 \pm 0.4\%$, $p < 0.05$, Fig. 5H). However, the effect of IBMX was not observed in the 6-OHDA-lesioned slices (no IBMX, $11.3 \pm 0.5\%$, IBMX, $10.7 \pm 0.4\%$, Fig. 5H and Table S1). This suggested an occlusion of the effect of IBMX by the lesion of DA neurons. The lack of effect of the PDE inhibitor specifically in D1R-responsive neurons, following 6-OHDA lesion could be explained by a decrease in PDE activity specifically in these neurons. This change in PDE activity is likely to contribute to the enhanced PKA activation in response to D1R or AC stimulation.

3.7. Spontaneous Ca^{2+} transient activity is increased in 6-OHDA-lesioned D1R-expressing striatal neurons

Intracellular Ca^{2+} increase has been implicated in ERK activation in many models ranging from *C. elegans* (Tomida et al., 2012) to CA1 pyramidal neurons in rodents (Zhai et al., 2013) and DA-denervated SPNs (Fieblinger et al., 2014a). Hence, we investigated intracellular free Ca^{2+} in striatal neurons of non-lesioned and 6-OHDA-lesioned mice using the biosensor GCaMP6s. We co-injected 6-OHDA or vehicle with an AAV expressing GCaMP6s (Chen et al., 2013) in the dorsal striatum of 4–6-week old mice, and 3–4 weeks later, acute striatal slices were imaged under a 2-photon microscope. In our experimental conditions, some SPNs were spontaneously active and showed transient increases in intracellular Ca^{2+} detected by the normalized fluorescence ratio ($\Delta F/F_0$). We therefore sorted the striatal neurons on the basis of their spontaneous activity during the baseline recording period into two categories, as described in the Methods section, spontaneously active and non-spontaneously active SPNs (Fig. 6A). The number of spontaneously active SPNs was higher in 6-OHDA-lesioned than in non-lesioned striata (non-lesioned, 13.1%, $n = 274/2085$, lesioned, 18.2%, $n = 319/1748$, $p < 0.001$, Fig. 6B). To determine whether this higher spontaneous activity affected dSPNs and/or iSPNs, we microinjected an AAV Cre-dependently expressing GCaMP6s (AAV-flex-GCaMP6s), into the striatum of *Drd1::Cre* (*D1Cre*) and *Adora2a::Cre* ($A2_A$ Cre) mice. In the 6-OHDA-lesioned *D1Cre* mice, cells expressing GCaMP6s were spontaneously more active than in the non-lesioned animals (non-lesioned, 11.3%, $n = 58/512$, lesioned, 19.7%, $n = 179/910$, $p < 0.001$, Fig. 6B). In contrast, in the $A2_A$ Cre mice, no significant difference was observed between lesioned and non-lesioned striata (non-lesioned 15.4%, $n = 80/518$, lesioned, 18.2%, $n = 69/379$, Fig. 6B). These results suggested that a higher proportion of dSPNs had spontaneous

Ca^{2+} activity in DA-depleted striatum.

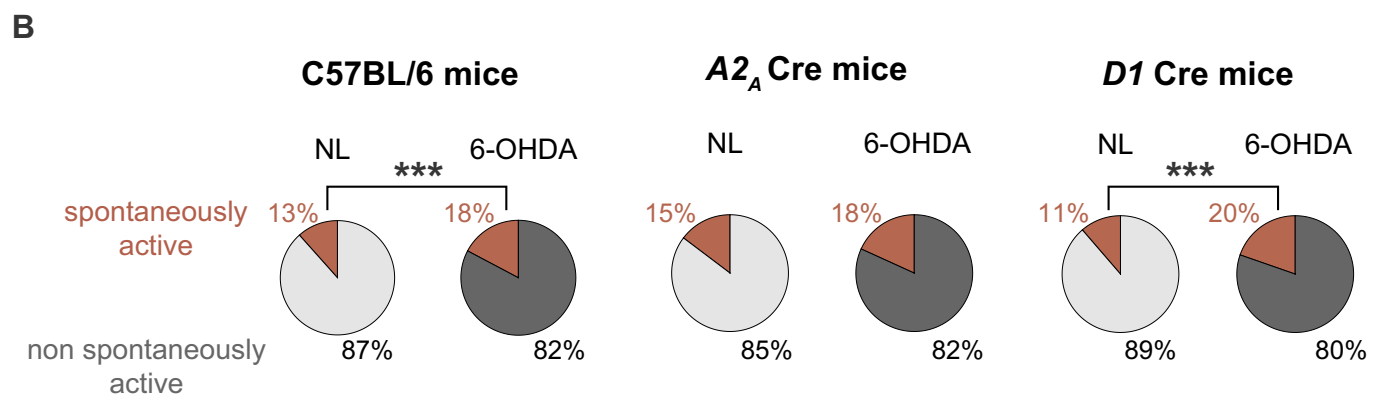
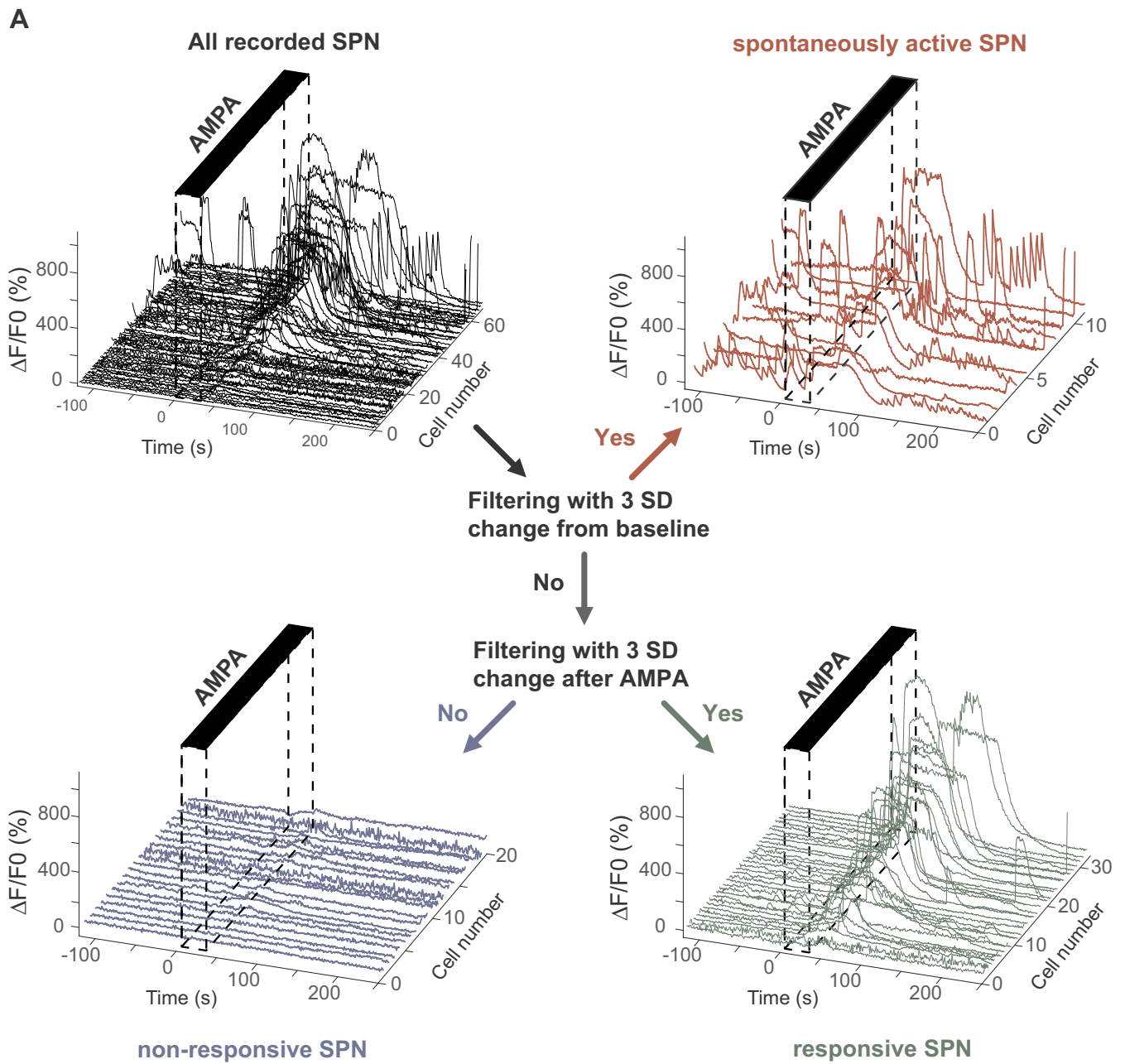
3.8. Specific enhancement of AMPA-induced intracellular Ca^{2+} dynamics in $A2_A$ R-expressing striatal neurons after 6-OHDA lesion

As mentioned above, co-application of AMPA and SKF81297 activated ERK in a larger number of neurons in the 6-OHDA-lesioned striatum than in the intact striatum (see Fig. 3B). These effects could be indicative of alterations in Ca^{2+} responses to AMPAR stimulation in the DA-denervated striatum. To address this question, we monitored intracellular Ca^{2+} dynamics following a 30 s AMPA (0.5 μ M) application in 6-OHDA-lesioned and control mice. We focused our analysis on the non-spontaneously active SPNs because spontaneous activity rendered the drug-induced Ca^{2+} responses difficult to evaluate. In the non-lesioned animals, AMPA-induced Ca^{2+} responses, evaluated by the normalized fluorescence ratio, were very variable from one neuron to another, but the average response was small (Fig. 7A middle panel). In contrast, in the 6-OHDA-lesioned animals, we observed a prolonged increase of the fluorescence ratio in response to AMPA application, showing an overall increase in Ca^{2+} responses (area under the curve [AUC]: non-lesioned $1.97 \pm 0.26 \times 10^3\%.s$, lesioned, $12.55 \pm 0.63 \times 10^3\%.s$, Fig. 7A right lower panel). When KCl (25 mM, 30 s) was applied at the end of all experiments, it produced a general and transient activation of virtually all neurons expressing GCaMP6s in the slices (Fig. 7A–C left panels). This stimulation allowed us to test the viability of striatal neurons in brain slices and also to determine the total number of responsive cells and, thus, the percentage of cells responsive to the application of AMPA. This calculation revealed a significant increase in the percentage of responsive cells following 6-OHDA lesion (non-lesioned 44.2%, $n = 206/466$, lesioned, and 61.2%, $n = 120/196$, Fig. 7A right upper panel).

To determine in which SPN population(s) the increase in AMPA-induced Ca^{2+} transients occurred in the DA-denervated striatum, we first microinjected AAV-flex-GCaMP6s into the striatum of *D1Cre* mice. In these mice the lesion did not modify the AMPA-induced increase in normalized fluorescence ratio (AUC: non-lesioned, $5.06 \pm 0.93 \times 10^3\%.s$, lesioned, $3.50 \pm 0.52 \times 10^3\%.s$, Fig. 7B right lower panel). In addition, the percentage of responsive cells was not changed (non-lesioned, 23.8%, $n = 62/261$, lesioned, 25.6%, $n = 103/403$, Fig. 7B right upper panel).

We then microinjected AAV-flex-GCaMP6s into the striatum of $A2_A$ Cre mice to selectively study the iSPNs. In these mice, AMPA markedly increased the normalized fluorescence ratio in 6-OHDA-lesioned compared to non-lesioned mice (AUC: non-lesioned, $7.62 \pm 1.04 \times 10^3\%.s$, lesioned, $18.38 \pm 3.14 \times 10^3\%.s$, Fig. 7C right lower panel). In addition, the percentage of AMPA-responsive iSPNs was strongly enhanced (non-lesioned, 57.8%, $n = 52/90$, lesioned, and 83.9%, $n = 47/56$, Fig. 7C right upper panel). These results indicated a pronounced iSPN-specific increase in AMPA-induced intracellular Ca^{2+} transients after 6-OHDA lesion.

In conclusion, this series of experiments shows that 6-OHDA lesion increases the amplitude of AMPA-induced Ca^{2+} responses and the



(caption on next page)

Fig. 6. Spontaneous Ca^{2+} transients are increased in D1R-expressing neurons of 6-OHDA-lesioned striatum.

(A) Sorting neurons based on their spontaneous activity and response to AMPA stimulation. Maximal change of normalized fluorescence ratio ($\Delta F/F_0$) of GCaMP6s biosensor was calculated for all the neurons in the field of view and all the time courses (All recorded SPNs) from different slices were plotted in 3D (one black line per neuron). Cells were separated in two groups based on the baseline activity. Cells were classified as spontaneously active if during baseline recording they presented a $\Delta F/F_0$ increase > 3 standard deviation (SD) calculated on the basal activity of all the cells (red curves). The other cells (non-spontaneously active) were further sorted according to their increase in $\Delta F/F_0$ after the application of AMPA. They were classified as responsive if they presented a $\Delta F/F_0$ increase > 3 SD after AMPA application (0.5 μM , 30 s, green curves) and as non-responsive if not (blue curves). (B) Comparison of the percentage of spontaneously active cells in non-lesioned (NL) and 6-OHDA-lesioned striatal slices. Left panel: wild type C57BL/6 mice injected with an AAV expressing GCaMP6s in all neurons. Middle panel: *Adora2A::Cre* (*A2A*Cre) mice injected with a Cre-dependent AAV (AAV-flex-GCaMP6s). Right panel: *Drd1::Cre* (*D1*Cre) mice injected with AAV-flex-GCaMP6s. Two-tailed Chi-square test (see Table S1), *** $p < 0.001$. (For interpretation of the references to colour in this figure legend, the reader is referred to the web version of this article.)

number of AMPA-responsive cells, and that this effect is selectively taking place in A2A_R -expressing cells, presumably iSPNs.

4. Discussion

Our work reveals the spatiotemporal dynamics of Ca^{2+} , PKA and ERK signaling using multiphoton biosensor imaging in the DA-denervated striatum of adult mice. Our results show that 6-OHDA lesion increases ERK and PKA activation in response to D1R stimulation. The increased activation of PKA results at least in part from an increase in $\text{G}\alpha_{\text{olf}}$ combined with a deficit in phosphodiesterase activity selectively in dSPNs. Monitoring Ca^{2+} signals revealed that the spontaneous Ca^{2+} transients are increased in D1R-expressing dSPNs of the DA-denervated striatum. In contrast, although their spontaneous activity is unchanged, the Ca^{2+} transients induced by stimulation of AMPA glutamate receptors in iSPNs are highly increased. Our work reveals distinct cell type-specific signaling alterations in the two populations of SPNs and suggests possible mechanisms for these alterations.

4.1. The activity of D1R- $\text{G}\alpha_{\text{olf}}$ -PKA pathway is increased in dSPNs after 6-OHDA lesion

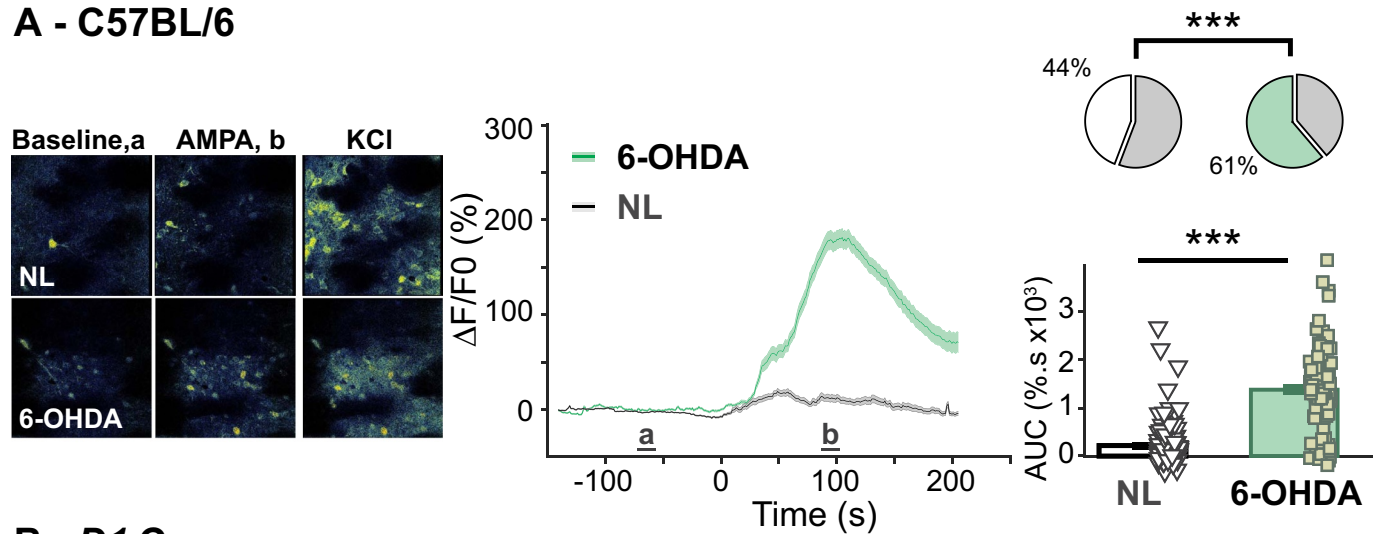
D1R signal transduction in SPNs is mediated by $\text{G}\alpha_{\text{olf}}$, the G protein that activates AC in these neurons (Corvol et al., 2001; Hervé et al., 1993; Zhuang et al., 2000). We found that after DA denervation the PKA response was specifically amplified in SPNs responsive to a D1R agonist, presumably dSPNs. Studies in transgenic mice expressing GFP under the control of the D1R gene promoter have shown that the D1-SPNs project to the *substantia nigra pars reticulata* and *globus pallidus pars interna* (reviews in Gerfen and Surmeier, 2011; Valjent et al., 2009). In contrast $< 1\%$ of striatonigral neurons express D2R (Matamales et al., 2009). However, in mice expressing GFP under the control of D1R promoter, a low GFP-positive innervation was also observed in the *globus pallidus pars externa* (Cazorla et al., 2014; Matamales et al., 2009) corresponding to axon collaterals of dSPNs (Cazorla et al., 2015; Parent et al., 2000). Finally, in the dorsal striatum the of SPNs expressing both D1Rs and D2Rs, is very low, $< 2\%$ (Gagnon et al., 2017). Therefore it is possible to conclude that, in the mouse dorsal striatum, D2-SPN are virtually exclusively iSPN while D1-SPNs are dSPNs but they can be a minor component of the indirect pathway, mostly as collateral projection.

The PKA pathway upregulation did not occur in the iSPNs since no modification of PKA signaling was observed after A2A_R stimulation. This can account for the previously reported enhanced phosphorylation of PKA substrates, DARPP-32 Thr-34 and GluA1 Ser-845, after acute administration of L-DOPA (Santini et al., 2007). Striatal levels of D1R (Hurley et al., 2001) and other mediators of D1R signaling (Girault et al., 1989) show no major modifications after DA denervation. In contrast, the levels of $\text{G}\alpha_{\text{olf}}$ are increased in the striatum of DA-denervated rodents and in postmortem samples from PD patients (Alcacer et al., 2012; Corvol et al., 2004; Ruiz-DeDiego et al., 2015). DA lesion selectively increases $\text{G}\alpha_{\text{olf}}$ amounts associated with D1Rs, leaving unaffected those associated with A2A_R s (Morigaki et al., 2017). Striatal $\text{G}\alpha_{\text{olf}}$ levels are regulated by DA and D1R utilization, presumably

through post-translational mechanisms (Hervé et al., 2001; Ruiz-DeDiego et al., 2015). In *Gnal^{+/-}* mice, which display a decrease of $\approx 50\%$ in $\text{G}\alpha_{\text{olf}}$ protein levels (Alcacer et al., 2012; Corvol et al., 2007), we found a decrease in PKA activation in response to D1R agonist confirming that $\text{G}\alpha_{\text{olf}}$ is a rate-limiting factor for the D1R-dependent cAMP/PKA pathway activation (Corvol et al., 2007). The PKA response to the D1R agonist was increased in 6-OHDA-lesioned *Gnal^{+/-}* mice as compared to non-lesioned mutant mice, but remained lower than in 6-OHDA-lesioned wild type mice, in agreement with previous biochemical results (Alcacer et al., 2012). Our present observations combined with previous results show that increased striatal $\text{G}\alpha_{\text{olf}}$ levels are an important factor leading to sensitized PKA responses to D1R stimulation in the DA-denervated striatum. Importantly, such $\text{G}\alpha_{\text{olf}}$ upregulation was detected in the putamen of PD patients (Corvol et al., 2004) showing that similar pathological processes occur in human. Our study identifies another factor contributing to enhanced cAMP signaling in dSPNs following DA lesion, namely a selective decrease in PDE activity. PDEs are a family of enzymes that degrade cAMP and/or cGMP, participate in the regulation of their intracellular levels, and directly contribute to the spatial and temporal dynamics of cAMP/PKA pathway in neurons (Castro et al., 2010; Gervasi et al., 2007, 2010). In adult striatal neurons, cAMP is constantly produced by ACs and degraded by PDEs since phosphodiesterase inhibition with IBMX enhances cAMP levels and activates PKA in both dSPNs and iSPNs, as revealed by an increase of AKAR3 FRET fluorescence in our study. In non-lesioned striatum a low concentration of IBMX (30 μM), devoid of effect by itself, enhanced AKAR3 signal in response to stimulation of D1R, A2A_R or AC. However, this effect was specifically lost in D1R-responsive neurons after DA denervation. A possible explanation of this loss is that the effects of 30 μM IBMX were occluded by a preexisting decrease in endogenous PDE activity. This putative decrease in PDE activity only occurred in D1R-expressing SPNs since the low concentration of PDE inhibitor remained effective in the A2A_R -expressing neurons of 6-OHDA-lesioned striatum, increasing the PKA responses to A2A_R agonist or forskolin. Several PDE families are expressed in the striatum, including PDE1, PDE4, and PDE10, and play a critical role in modulating cAMP-mediated DA signaling. Knockout of PDE1B in mice increases locomotor activity and responses to DA agonists (Ehrman et al., 2006), but in 6-OHDA-lesioned mice an upregulation of PDE1B was reported (Sancesario et al., 2004). In contrast, studies in PD patients point to a reduced expression of PDE10A which correlates with PD duration and severity of motor symptoms (Niccolini et al., 2015) and a decrease in PDE4 (Niccolini et al., 2017). However, in the striatum, PDE4 is predominantly active in DA terminals, regulating TH phosphorylation (Nishi et al., 2008). The improvement observed in PD following treatment with a PDE4 inhibitor (Rolipram) was attributed to a protective effect on DA neuron degeneration (Yang et al., 2008). In rodents, PDE10A mRNA and protein levels are decreased in 6-OHDA-lesioned striatum (Giorgi et al., 2008). This reduction in PDE10A levels is associated with higher cAMP-dependent phosphorylation in response to D1R stimulation (Mango et al., 2014). Thus, decreased PDE10A activity is a strong candidate to explain our observations and further work is needed to test this hypothesis.

Although not investigated in the present study, changes in ACs may

A - C57BL/6



B - D1 Cre

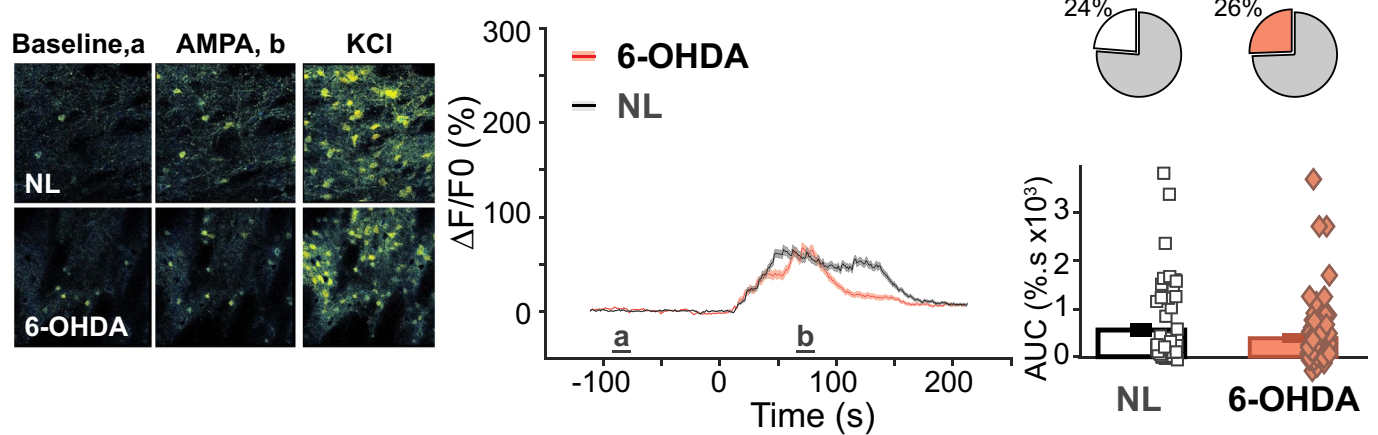
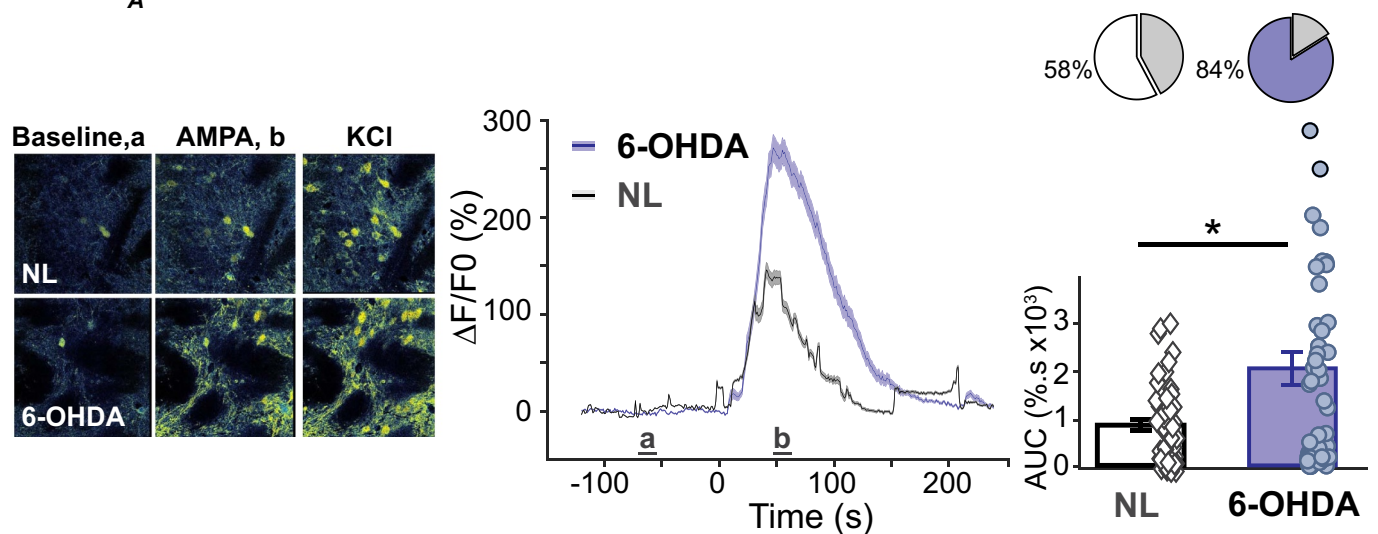
C - A2_A Cre

Fig. 7. Specific upregulation of AMPA-induced intracellular Ca^{2+} dynamics in $\text{A2}_A\text{R}$ -expressing neurons in 6-OHDA-lesioned striatum. Intracellular Ca^{2+} increase after AMPA application in non-spontaneously active cells (see Fig. 6A) measured with GCaMP6s biosensor in striatal slices of non-lesioned (NL) and 6-OHDA-lesioned (6-OHDA) mice. (A) Wild type C57Bl/6 mice expressing GCaMP6s in all neurons. Left panel: representative pseudocolor-coded images representing $\Delta F/F0$ during the baseline (a), after AMPA (0.5 μM , 30 s, b), and then KCl (25 mM) application. Middle panel: time course of AMPA-induced intracellular Ca^{2+} dynamics in non-lesioned and 6-OHDA-lesioned striatal slices. a and b indicate the time at which left panel pictures were taken. Right upper panel: Percentage of responsive cells, test two-tailed Chi-square see (Table S1). Right lower panel: area under the curve (AUC) of Ca^{2+} responses in striatal neurons after application of AMPA (0.5 μM , 30 s), Mann-Whitney test, see Table S1. (B) Same as in A, in *Drd1::Cre* mice (D1Cre) injected with a Cre-dependent AAV (AAV-flex-GCaMP6s) (see Table S1 for statistical analysis). (C) Same as in A, in *Adora2A::Cre* mice ($\text{A2}_A\text{Cre}$) injected with AAV-flex-GCaMP6s. (see Table S1 for statistical analysis). (A-C) * $p < 0.05$, ** $p < 0.01$, *** $p < 0.001$.

also contribute to the increased cAMP responses in DA-lesioned mice. Among the ten different ACs, AC5 is the most abundant subtype in the striatum (Iwamoto et al., 2004). Work in rat showed that DA denervation increases activity and expression of AC5 in the striatum (Rangel-Barajas et al., 2011). In conclusion, the combination of several alterations, including increases in $G\alpha_{olf}$ and AC5 and decrease in PDE activity may account for the increased responsiveness of the PKA pathway in D1R-expressing SPNs following dopaminergic lesion.

4.2. Differential changes in intracellular Ca^{2+} transients in SPNs after 6-OHDA lesion

In this study, we observed that in DA-denervated striatal slices SPNs displayed more spontaneous intracellular Ca^{2+} transients than in non-lesioned slices, a modification that occurred predominantly in dSPNs. It has been previously shown that spontaneous Ca^{2+} transients and firing rate of SPNs are enhanced after DA denervation (Jáidar et al., 2010), without identification of the SPN population. This increased activity could be linked to the elevated intrinsic excitability of dSPN after 6-OHDA lesion, attributed to a possible homeostatic response to the loss of excitatory D1R signaling (Fieblinger et al., 2014b; Suárez et al., 2014; Suarez et al., 2016, 2018). It is noteworthy that the intrinsic excitability is higher in iSPNs than in dSPNs in basal conditions, which correlates with a more frequent occurrence of Ca^{2+} transients in iSPNs than in dSPNs observed in the non-lesioned striata (Gertler et al., 2008). It was proposed that DA denervation reduces this difference between excitability of dSPNs and iSPNs, mostly by increasing dSPN excitability (Maurice et al., 2015). Accordingly, in our experiments the proportions of spontaneously active neurons in the dSPN and iSPN populations appeared to equalize following DA denervation.

The increased spontaneous activity of dSPNs in ex vivo corticostriatal slices contrasts with in vivo observations. A recent study reported that following 6-OHDA lesion, dSPN activity in awake mice was decreased while iSPN activity was increased when animals were immobile (Ryan et al., 2018). These observations confirmed and expanded previous reports in anesthetized rodents (Mallet et al., 2006). The increased basal activity of iSPNs in vivo is attributed to their enhanced sensitivity to cortical inputs (Escande et al., 2016; Mallet et al., 2006; Ryan et al., 2018). In our slice study we observed an increase in AMPA-induced intracellular Ca^{2+} responses specifically in iSPNs of lesioned mice, without change in dSPN. These findings are in agreement with several works that identified corticostriatal synaptic reorganization following lesion of DA neurons. Indeed, DA denervation induces a pruning of cortical synapses associated with an increase of dendritic excitability specifically in iSPN, resulting in an enhancement of the average amplitude of corticostriatal synaptic responses (Fieblinger et al., 2014b). iSPNs express functional Ca^{2+} -permeable AMPA receptors at corticostriatal synapses and AMPA receptor subunit phosphorylation, trafficking, and alternative splicing are enhanced in animal models of PD, possibly contributing to an enhanced function of AMPA receptors (Ba et al., 2011; Kobylecki et al., 2013). These various modifications could provide potential mechanisms for the enhancement of AMPA-induced intracellular Ca^{2+} transients we observed in iSPNs. Increased Ca^{2+} transients can have numerous impacts on neuronal function including regulation of synaptic strength, cellular excitability, and gene expression, as well as modulation of calcium-activated potassium channels that control the duration and intervals of action potentials (Trusel et al., 2015). Synaptic plasticity in iSPN has been shown to be calcium-dependent (Trusel et al., 2015). Inflammation increases AMPA responses through Ca^{2+} -permeable AMPA receptors and voltage-gated calcium channels specifically in iSPNs of the dorsal striatum (Winland et al., 2017). Since DA lesion triggers an inflammatory response (Cicchetti et al., 2002), it will be important to examine its contribution to the altered responsiveness of iSPNs.

It is remarkable that although our understanding of the basal ganglia circuits is much more complete and complex than it was

30 years ago, the in vivo results in 6-OHDA-lesioned mice as well as our observations in slices are consistent with the model proposed for primates by DeLong in which the loss of striatal DA resulted in an increase in transmission through the indirect pathway (DeLong, 1990).

4.3. ERK activity is increased after 6-OHDA lesion

Phosphorylation of ERK is triggered in neurons by various external stimuli, including neurotransmitters and growth factors, leading to a wide range of plastic responses through activation of cytosolic and nuclear targets [review in (Girault, 2012)]. In the striatum ERK activation is essential for instrumental learning (Shiflett et al., 2010) and long-lasting effects of addictive drugs (Valjent et al., 2000). Conditional deletion of ERK1/2 in dSPNs or iSPNs induces pathway-specific alterations in motor function, synaptic properties, and plasticity-related gene expression, emphasizing the importance of ERK for SPNs function (Hutton et al., 2017). In non-lesioned animals D1R activation leads to a modest activation of ERK in SPNs (Fieblinger et al., 2014a; Gerfen et al., 2002). In contrast, in DA-lesioned mice, treatment with D1R agonists or L-DOPA results in pronounced and sustained activation of ERK that depends on the canonical PKA signaling pathway and MEK1/2 (Gerfen et al., 2002; Darmopil et al., 2009; Fieblinger et al., 2014a; Pavón et al., 2006; Santini et al., 2007). Our imaging experiments with ERK biosensor confirm the limited responses to D1R agonist in non-lesioned striata and the upregulation of ERK responses after 6-OHDA lesion. ERK activation was detected in close to half of the cells in both conditions indicating that in the DA-denervated striatum, the increase in D1R-induced ERK responses is mostly attributable to an increased response in a specific set of SPNs, and not to the recruitment of additional SPNs. In hippocampal neurons, ERK can be activated after glutamate receptor stimulation through increases in intracellular calcium (Zhai et al., 2013). In the striatum, we showed that pharmacological AMPA receptor stimulation, mimicking cortical or thalamic glutamatergic inputs, can also activate ERK in a small population of SPNs. This is in agreement with previous reports showing that excitatory glutamatergic synaptic transmission and corticostriatal stimulation activate ERK in the striatum, mainly in iSPNs (Gerfen et al., 2002; Sgambato et al., 1998). AMPA-induced ERK activation was increased after DA-denervation. Since our imaging study indicated that AMPA-induced intracellular Ca^{2+} increase was limited to iSPN after 6-OHDA lesion, we can hypothesize that ERK activation by AMPA is due to Ca^{2+} increase in these neurons. This hypothesis is in line with previous findings by Gerfen and colleagues who found that after DA-denervation, corticostriatal stimulation elicited ERK activation in iSPN, identified by histochemical localization of enkephalin mRNA (Gerfen et al., 2002). In D1R-expressing dSPNs, Ca^{2+} and cAMP signaling pathways synergize to activate ERK in response to addictive drugs and, possibly in physiological circumstances, leading to long-term changes (Girault et al., 2007), including modification of neuronal excitability, changes in activity-induced gene expression and modulation of dendritic spine density (Cerovic et al., 2013). In our experiments, the combination of D1R and AMPA receptor agonists, produced an ERK activation of comparable amplitude as the D1R agonist alone, in non-lesioned or DA-denervated mice. This is in agreement with data indicating that D1R agonist-induced activation of ERK signaling in DA-denervated striatum is not completely depending on ionotropic glutamate receptors (Fieblinger et al., 2014a; Gerfen et al., 2002). However, the use of ERK imaging at the single cell level allowed us to detect an increase in the number of responsive cells. When AMPA and D1R agonist were co-applied, ERK was activated in 43% of the SPNs in the non-lesioned striatum and 67% after 6-OHDA lesion. This result implies that ERK activation took place in the two SPN populations after 6-OHDA lesion.

5. Conclusions

Our work using 2-photon biosensor imaging in the DA-denervated

striatum of adult mice underlines the complex signaling dysregulations in SPNs in the absence of DA inputs. It reveals distinct cell type-specific alterations of cAMP, Ca²⁺ and ERK responses in the two populations of SPNs. These results emphasize the need to take into consideration these differences for the development of treatments in PD and the importance of acting both dSPNs and iSPNs for the normalization of signaling pathway dynamics after DA denervation.

Supplementary data to this article can be found online at <https://doi.org/10.1016/j.nbd.2019.104506>.

Funding

The present work was supported in part by Inserm and Sorbonne University, by ERC-2009-AdG_20090506, FRM DEQ20081213971, and CRCNS/ANR 1515686 to JAG and ANR09-MNPS-014, ANR-16-CE37-0003-01 AMEDYST and France Parkinson to DH. LLM was supported by L'Oréal-UNESCO - Bourse française *Pour les Femmes et la Science*, *Journées de Neurologie de Langue Française* and French Society of Neurology, and a poste d'accueil INSERM.

Author contributions

L.L.M., J.A.G., D.H., and N.G. designed the experiments. L.L.M. conducted the toxin and AAV injections. L.L.M., N.G., conducted the two-photon experiments and the analysis; and L.L.M. and S.L. conducted the immunoblot experiments. L.L.M., J.A.G., D.H., and N.G. wrote the paper.

Competing interests

No competing interests.

Acknowledgments

We thank Pierre Vincent, Regine Hepp, Karel Svoboda, Olivier Pertz, Jun-ichi Miyazaki, Michiyuki Matsuda, Jin Zhang and Ted Abel for providing viruses and plasmids, Alban de Kerchove d'Exaerde for providing *Adora2A::Cre* mice. We thank the cell and tissue imaging facility of the *Institut du Fer à Moulin*, where all image acquisition and analysis have been performed.

References

- Albin, R.L., Young, A.B., Penney, J.B., 1989. The functional anatomy of basal ganglia disorders. *Trends Neurosci.* 12, 366–375.
- Alcacer, C., Santini, E., Valjent, E., Gaven, F., Girault, J.-A., Hervé, D., 2012. Gα(olf) mutation allows parsing the role of cAMP-dependent and extracellular signal-regulated kinase-dependent signaling in L-3,4-dihydroxyphenylalanine-induced dyskinesia. *J. Neurosci.* 32, 5900–5910.
- Alcacer, C., Andreoli, L., Sebastianutto, L., Jakobsson, J., Fieblinger, T., Cenci, M.A., 2017. Chemogenetic stimulation of striatal projection neurons modulates responses to Parkinson's disease therapy. *J. Clin. Invest.* 127, 720–734.
- Allen, M.D., Zhang, J., 2006. Subcellular dynamics of protein kinase A activity visualized by FRET-based reporters. *Biochem. Biophys. Res. Commun.* 348, 716–721.
- Ba, M., Kong, M., Yu, G., Sun, X., Liu, Z., Wang, X., 2011. GluR1 phosphorylation and persistent expression of levodopa-induced motor response alterations in the Hemiparkinsonian rat. *Neurochem. Res.* 36, 1135–1144.
- Belluscio, L., Gold, G.H., Nemes, A., Axel, R., 1998. Mice deficient in G(olf) are anosmic. *Neuron* 20, 69–81.
- Bertran-Gonzalez, J., Bosch, C., Maroteaux, M., Matamalas, M., Hervé, D., Valjent, E., Girault, J.-A., 2008. Opposing patterns of signaling activation in dopamine D1 and D2 receptor-expressing striatal neurons in response to cocaine and haloperidol. *J. Neurosci.* 28, 5671–5685.
- Castro, L.R.V., Gervasi, N., Guiot, E., Cavellini, L., Nikolaeva, V.O., Paupardin-Tritsch, D., Vincent, P., 2010. Type 4 phosphodiesterase plays different integrating roles in different cellular domains in pyramidal cortical neurons. *J. Neurosci.* 30, 6143–6151.
- Castro, L.R.V., Brito, M., Guiot, E., Polito, M., Korn, C.W., Hervé, D., Girault, J.-A., Paupardin-Tritsch, D., Vincent, P., 2013. Striatal neurones have a specific ability to respond to phasic dopamine release. *J. Physiol. Lond.* 591, 3197–3214.
- Cazorla, M., de Carvalho, F.D., Chohan, M.O., Shegda, M., Chuhma, N., Rayport, S., Ahmari, S.E., Moore, H., Kellendonk, C., 2014. Dopamine D2 receptors regulate the anatomical and functional balance of basal ganglia circuitry. *Neuron* 81, 153–164.
- Cazorla, M., Kang, U.J., Kellendonk, C., 2015. Balancing the basal ganglia circuitry: a possible new role for dopamine D2 receptors in health and disease. *Mov. Disord.* 30, 895–903.
- Cerovic, M., d'Isa, R., Tonini, R., Brambilla, R., 2013. Molecular and cellular mechanisms of dopamine-mediated behavioral plasticity in the striatum. *Neurobiol. Learn. Mem.* 105, 63–80.
- Chen, T.-W., Wardill, T.J., Sun, Y., Pulver, S.R., Renninger, S.L., Baohan, A., Schreier, E.R., Kerr, R.A., Orger, M.B., Jayaraman, V., et al., 2013. Ultrasensitive fluorescent proteins for imaging neuronal activity. *Nature* 499, 295–300.
- Cicchetti, F., Brownell, A.L., Williams, K., Chen, Y.L., Livni, E., Isacson, O., 2002. Neuroinflammation of the nigrostriatal pathway during progressive 6-OHDA dopamine degeneration in rats monitored by immunohistochemistry and PET imaging. *Eur. J. Neurosci.* 15, 991–998.
- Corvol, J.C., Studler, J.M., Schonn, J.S., Girault, J.A., Hervé, D., 2001. Galphao(olf) is necessary for coupling D1 and A2a receptors to adenylyl cyclase in the striatum. *J. Neurochem.* 76, 1585–1588.
- Corvol, J.-C., Muriel, M.-P., Valjent, E., Féger, J., Hanoune, N., Girault, J.-A., Hirsch, E.C., Hervé, D., 2004. Persistent increase in olfactory type G-protein alpha subunit levels may underlie D1 receptor functional hypersensitivity in Parkinson disease. *J. Neurosci.* 24, 7007–7014.
- Corvol, J.-C., Valjent, E., Pascoli, V., Robin, A., Stipanovich, A., Luedtke, R.R., Belluscio, L., Girault, J.-A., Hervé, D., 2007. Quantitative changes in Galphao(olf) protein levels, but not D1 receptor, alter specifically acute responses to psychostimulants. *Neuropsychopharmacology* 32, 1109–1121.
- Darmopil, S., Martín, A.B., De Diego, I.R., Ares, S., Moratalla, R., 2009. Genetic inactivation of dopamine D1 but not D2 receptors inhibits L-DOPA-induced dyskinesia and histone activation. *Biol. Psychiatry* 66, 603–613.
- DeLong, M.R., 1990. Primate models of movement disorders of basal ganglia origin. *Trends Neurosci.* 13, 281–285.
- Durieux, P.F., Bearzatto, B., Guiducci, S., Buch, T., Waisman, A., Zoli, M., Schiffmann, S.N., de Kerchove d'Exaerde, A., 2009. D2R striatopallidal neurons inhibit both locomotor and drug reward processes. *Nat. Neurosci.* 12, 393–395.
- Ehrman, L.A., Williams, M.T., Schaefer, T.L., Gudelsky, G.A., Reed, T.M., Fienberg, A.A., Greengard, P., Vorhees, C.V., 2006. Phosphodiesterase 1B differentially modulates the effects of methamphetamine on locomotor activity and spatial learning through DARPP32-dependent pathways: evidence from PDE1B-DARPP32 double-knockout mice. *Genes Brain Behav.* 5, 540–551.
- Escande, M.V., Taravini, I.R.E., Zold, C.L., Belforte, J.E., Murer, M.G., 2016. Loss of homeostasis in the direct pathway in a mouse model of asymptomatic Parkinson's disease. *J. Neurosci.* 36, 5686–5698.
- Fieblinger, T., Sebastianutto, I., Alcacer, C., Bimpisidis, Z., Maslava, N., Sandberg, S., Engblom, D., Cenci, M.A., 2014a. Mechanisms of dopamine D1 receptor-mediated ERK1/2 activation in the parkinsonian striatum and their modulation by metabotropic glutamate receptor type 5. *J. Neurosci.* 34, 4728–4740.
- Fieblinger, T., Graves, S.M., Sebel, L.E., Alcacer, C., Plotkin, J.L., Gertler, T.S., Chan, C.S., Heiman, M., Greengard, P., Cenci, M.A., et al., 2014b. Cell type-specific plasticity of striatal projection neurons in parkinsonism and L-DOPA-induced dyskinesia. *Nat. Commun.* 5, 5316.
- Fritz, R.D., Zeltzer, M., Reimann, A., Martin, K., Fusco, L., Ritsma, L., Ponsioen, B., Fluri, E., Schulte-Merker, S., van Rheenen, J., et al., 2013. A versatile toolkit to produce sensitive FRET biosensors to visualize signaling in time and space. *Sci. Signal.* 6 (rs12).
- Gagnon, D., Petryszyn, S., Sanchez, M.G., Bories, C., Beaulieu, J.M., De Koninck, Y., Parent, A., Parent, M., 2017. Striatal neurons expressing D1 and D2 receptors are morphologically distinct and differently affected by dopamine denervation in mice. *Sci. Rep.* 7, 41432.
- Gerfen, C.R., Surmeier, D.J., 2011. Modulation of striatal projection systems by dopamine. *Annu. Rev. Neurosci.* 34, 441–466.
- Gerfen, C.R., Engber, T.M., Mahan, L.C., Susel, Z., Chase, T.N., Monsma, F.J., Sibley, D.R., 1990. D1 and D2 dopamine receptor-regulated gene expression of striatonigral and striatopallidal neurons. *Science* 250, 1429–1432.
- Gerfen, C.R., Miyachi, S., Paletzki, R., Brown, P., 2002. D1 dopamine receptor super-sensitivity in the dopamine-depleted striatum results from a switch in the regulation of ERK1/2/MAP kinase. *J. Neurosci.* 22, 5042–5054.
- Gertler, T.S., Chan, C.S., Surmeier, D.J., 2008. Dichotomous anatomical properties of adult striatal medium spiny neurons. *J. Neurosci.* 28, 10814–10824.
- Gervasi, N., Hepp, R., Tricoire, L., Zhang, J., Lambolze, B., Paupardin-Tritsch, D., Vincent, P., 2007. Dynamics of protein kinase A signaling at the membrane, in the cytosol, and in the nucleus of neurons in mouse brain slices. *J. Neurosci.* 27, 2744–2750.
- Gervasi, N., Tchénio, P., Preat, T., 2010. PKA dynamics in a Drosophila learning center: coincidence detection by rutabaga adenylyl cyclase and spatial regulation by dunce phosphodiesterase. *Neuron* 65, 516–529.
- Giorgi, M., D'Angelo, V., Esposito, Z., Luccetelli, V., Sorge, R., Martorana, A., Stefani, A., Bernardi, G., Sancesario, G., 2008. Lowered cAMP and cGMP signalling in the brain during levodopa-induced dyskinesias in hemiparkinsonian rats: new aspects in the pathogenetic mechanisms. *Eur. J. Neurosci.* 28, 941–950.
- Girault, J.-A., 2012. Integrating neurotransmission in striatal medium spiny neurons. *Adv. Exp. Med. Biol.* 970, 407–429.
- Girault, J.A., Raisman-Vozari, R., Agid, Y., Greengard, P., 1989. Striatal phosphoproteins in Parkinson disease and progressive supranuclear palsy. *Proc. Natl. Acad. Sci. U. S. A.* 86, 2493–2497.
- Girault, J.-A., Valjent, E., Caboche, J., Hervé, D., 2007. ERK2: a logical AND gate critical for drug-induced plasticity? *Curr. Opin. Pharmacol.* 7, 77–85.
- Gong, S., Doughty, M., Harbaugh, C.R., Cummins, A., Hatten, M.E., Heintz, N., Gerfen, C.R., 2007. Targeting Cre recombinase to specific neuron populations with bacterial artificial chromosome constructs. *J. Neurosci.* 27, 9817–9823.

- Harvey, C.D., Ehrhardt, A.G., Cellurale, C., Zhong, H., Yasuda, R., Davis, R.J., Svoboda, K., 2008. A genetically encoded fluorescent sensor of ERK activity. *Proc. Natl. Acad. Sci. U. S. A.* 105, 19264–19269.
- Heckman, P.R.A., Blokland, A., Bollen, E.P.P., Prickaerts, J., 2018. Phosphodiesterase inhibition and modulation of corticostriatal and hippocampal circuits: clinical overview and translational considerations. *Neurosci. Biobehav. Rev.* 87, 233–254.
- Hervé, D., 2011. Identification of a specific assembly of the g protein *golf* as a critical and regulated module of dopamine and adenosine-activated cAMP pathways in the striatum. *Front. Neuroanat.* 5, 48.
- Hervé, D., Lévi-Strauss, M., Marey-Semper, I., Verney, C., Tassin, J.P., Glowinski, J., Girault, J.A., 1993. G(olf) and Gs in rat basal ganglia: possible involvement of G(olf) in the coupling of dopamine D1 receptor with adenylyl cyclase. *J. Neurosci.* 13, 2237–2248.
- Hervé, D., Le Moine, C., Corvol, J.C., Belluscio, L., Ledent, C., Fienberg, A.A., Jaber, M., Studler, J.M., Girault, J.A., 2001. Galpha(olf) levels are regulated by receptor usage and control dopamine and adenosine action in the striatum. *J. Neurosci.* 21, 4390–4399.
- Hurley, M.J., Mash, D.C., Jenner, P., 2001. Dopamine D(1) receptor expression in human basal ganglia and changes in Parkinson's disease. *Brain Res. Mol. Brain Res.* 87, 271–279.
- Hutton, S.R., Otis, J.M., Kim, E.M., Lamsal, Y., Stuber, G.D., Snider, W.D., 2017. ERK/MAPK signaling is required for pathway-specific striatal motor functions. *J. Neurosci.* 37, 8102–8115.
- Iwamoto, T., Iwatsubo, K., Okumura, S., Hashimoto, Y., Tsunematsu, T., Toya, Y., Hervé, D., Umemura, S., Ishikawa, Y., 2004. Disruption of type 5 adenylyl cyclase negates the developmental increase in Galphaolf expression in the striatum. *FEBS Lett.* 564, 153–156.
- Jáidar, O., Carrillo-Reid, L., Hernández, A., Drucker-Colín, R., Bargas, J., Hernández-Cruz, A., 2010. Dynamics of the Parkinsonian striatal microcircuit: entrainment into a dominant network state. *J. Neurosci.* 30, 11326–11336.
- Kawaguchi, Y., Wilson, C.J., Emsen, P.C., 1989. Intracellular recording of identified neostriatal patch and matrix spiny cells in a slice preparation preserving cortical inputs. *J. Neurophysiol.* 62, 1052–1068.
- Kobylecki, C., Crossman, A.R., Ravenscroft, P., 2013. Alternative splicing of AMPA receptor subunits in the 6-OHDA-lesioned rat model of Parkinson's disease and L-DOPA-induced dyskinesia. *Exp. Neurol.* 247, 476–484.
- Komatsu, N., Aoki, K., Yamada, M., Yukinaga, H., Fujita, Y., Kamioka, Y., Matsuda, M., 2011. Development of an optimized backbone of FRET biosensors for kinases and GTPases. *Mol. Biol. Cell* 22, 4647–4656.
- Kravitz, A.V., Freeze, B.S., Parker, P.R.L., Kay, K., Thwin, M.T., Deisseroth, K., Kreitzer, A.C., 2010. Regulation of parkinsonian motor behaviours by optogenetic control of basal ganglia circuitry. *Nature* 466, 622–626.
- Luczak, V., Blackwell, K.T., Abel, T., Girault, J.-A., Gervasi, N., 2017. Dendritic diameter influences the rate and magnitude of hippocampal cAMP and PKA transients during β -adrenergic receptor activation. *Neurobiol. Learn. Mem.* 138, 10–20.
- Mallet, N., Ballion, B., Le Moine, C., Gonon, F., 2006. Cortical inputs and GABA interneurons imbalance projection neurons in the striatum of parkinsonian rats. *J. Neurosci.* 26, 3875–3884.
- Mango, D., Bonito-Oliva, A., Ledonne, A., Nisticò, R., Castelli, V., Giorgi, M., Sancesario, G., Fisone, G., Berretta, N., Mercuri, N.B., 2014. Phosphodiesterase 10A controls D1-mediated facilitation of GABA release from striato-nigral projections under normal and dopamine-depleted conditions. *Neuropharmacology* 76 (Pt A), 127–136.
- Matamales, M., Bertran-Gonzalez, J., Salomon, L., Degos, B., Deniau, J.-M., Valjent, E., Hervé, D., Girault, J.-A., 2009. Striatal medium-sized spiny neurons: identification by nuclear staining and study of neuronal subpopulations in BAC transgenic mice. *PLoS ONE* 4, e4770.
- Maurice, N., Liberge, M., Jaouen, F., Ztaou, S., Hanini, M., Camon, J., Deisseroth, K., Amalric, M., Kerkerian-Le Goff, L., Beurrier, C., 2015. Striatal cholinergic interneurons control motor behavior and basal ganglia function in experimental parkinsonism. *Cell Rep.* 13, 657–666.
- Morigaki, R., Okita, S., Goto, S., 2017. Dopamine-induced changes in Gaolf protein levels in Striatonigral and Striatopallidal medium spiny neurons underlie the genesis of L-DOPA-induced dyskinesia in parkinsonian mice. *Front. Cell. Neurosci.* 11, 26.
- Niccolini, F., Foltynie, T., Reis Marques, T., Muhlert, N., Tziortzi, A.C., Searle, G.E., Natesan, S., Kapur, S., Rabiner, E.A., Gunn, R.N., et al., 2015. Loss of phosphodiesterase 10A expression is associated with progression and severity in Parkinson's disease. *Brain* 138, 3003–3015.
- Niccolini, F., Wilson, H., Pagano, G., Coello, C., Mehta, M.A., Searle, G.E., Gunn, R.N., Rabiner, E.A., Foltynie, T., Politis, M., 2017. Loss of phosphodiesterase 4 in Parkinson disease: relevance to cognitive deficits. *Neurology* 89, 586–593.
- Nishi, A., Kuroiwa, M., Miller, D.B., O'Callaghan, J.P., Bateup, H.S., Shuto, T., Sotogaku, N., Fukuda, T., Heintz, N., Greengard, P., et al., 2008. Distinct roles of PDE4 and PDE10A in the regulation of cAMP/PKA signaling in the striatum. *J. Neurosci.* 28, 10460–10471.
- Parent, A., Sato, F., Wu, Y., Gauthier, J., Lévesque, M., Parent, M., 2000. Organization of the basal ganglia: the importance of axonal collateralization. *Trends Neurosci.* 23, S20–S27.
- Pavón, N., Martín, A.B., Mendiola, A., Moratalla, R., 2006. ERK phosphorylation and FosB expression are associated with L-DOPA-induced dyskinesia in hemiparkinsonian mice. *Biol. Psychiatry* 59, 64–74.
- Polito, M., Guiot, E., Gangarossa, G., Longueville, S., Doulazmi, M., Valjent, E., Hervé, D., Girault, J.-A., Paupardin-Tritsch, D., Castro, L.R.V., et al., 2015. Selective effects of PDE10A inhibitors on Striatopallidal neurons require phosphatase inhibition by DARPP-32. *ENeuro* 2.
- Rangel-Barajas, C., Silva, I., Lopéz-Santiago, L.M., Aceves, J., Erlj, D., Florán, B., 2011. L-DOPA-induced dyskinesia in hemiparkinsonian rats is associated with up-regulation of adenylyl cyclase type V/VI and increased GABA release in the substantia nigra reticulata. *Neurobiol. Dis.* 41, 51–61.
- Redgrave, P., Rodriguez, M., Smith, Y., Rodriguez-Oroz, M.C., Lehericy, S., Bergman, H., Agid, Y., DeLong, M.R., Obeso, J.A., 2010. Goal-directed and habitual control in the basal ganglia: implications for Parkinson's disease. *Nat. Rev. Neurosci.* 11, 760–772.
- Ruiz-DeDiego, I., Naranjo, J.R., Hervé, D., Moratalla, R., 2015. Dopaminergic regulation of olfactory type G-protein α subunit expression in the striatum. *Mov. Disord.* 30, 1039–1049.
- Ryan, M.B., Bair-Marshall, C., Nelson, A.B., 2018. Aberrant striatal activity in parkinsonism and levodopa-induced dyskinesia. *Cell Rep.* 23, 3438–3446 (e5).
- Sancesario, G., Giorgi, M., D'Angelo, V., Modica, A., Martorana, A., Morello, M., Bengtson, C.P., Bernardi, G., 2004. Down-regulation of nitric transmission in the rat striatum after chronic nigrostriatal deafferentation. *Eur. J. Neurosci.* 20, 989–1000.
- Santini, E., Valjent, E., Usiello, A., Carta, M., Borgkvist, A., Girault, J.-A., Hervé, D., Greengard, P., Fisone, G., 2007. Critical involvement of cAMP/DARPP-32 and extracellular signal-regulated protein kinase signaling in L-DOPA-induced dyskinesia. *J. Neurosci.* 27, 6995–7005.
- Schiffmann, S.N., Vanderhaeghen, J.J., 1993. Adenosine A2 receptors regulate the gene expression of striatopallidal and striatonigral neurons. *J. Neurosci.* 13, 1080–1087.
- Sgambato, V., Pagès, C., Rogard, M., Besson, M.J., Caboche, J., 1998. Extracellular signal-regulated kinase (ERK) controls immediate early gene induction on corticostriatal stimulation. *J. Neurosci.* 18, 8814–8825.
- Shiflett, M.W., Brown, R.A., Balleine, B.W., 2010. Acquisition and performance of goal-directed instrumental actions depends on ERK signaling in distinct regions of dorsal striatum in rats. *J. Neurosci.* 30, 2951–2959.
- Suárez, L.M., Solís, O., Caramés, J.M., Taravini, I.R., Solís, J.M., Murer, M.G., Moratalla, R., 2014. L-DOPA treatment selectively restores spine density in dopamine receptor D2-expressing projection neurons in dyskinetic mice. *Biol. Psychiatry* 75, 711–722.
- Suarez, L.M., Solís, O., Aguado, C., Lujan, R., Moratalla, R., 2016. L-DOPA oppositely regulates synaptic strength and spine morphology in D1 and D2 striatal projection neurons in dyskinesia. *Cereb. Cortex* 26, 4253–4264.
- Suarez, L.M., Alberquilla, S., García-Montes, J.R., Moratalla, R., 2018. Differential synaptic remodeling by dopamine in direct and indirect striatal projection neurons in *pitx3* mice, a genetic model of Parkinson's disease. *J. Neurosci.* 38, 3619–3630.
- Tomida, T., Oda, S., Takekawa, M., Iino, Y., Saito, H., 2012. The temporal pattern of stimulation determines the extent and duration of MAPK activation in a *Caenorhabditis elegans* sensory neuron. *Sci. Signal* 5 (ra76).
- Trusel, M., Cavaccini, A., Gritti, M., Greco, B., Saintot, P.-P., Nazzaro, C., Cerovic, M., Morella, I., Brambilla, R., Tonini, R., 2015. Coordinated regulation of synaptic plasticity at striatopallidal and striatonigral neurons orchestrates motor control. *Cell Rep.* 13, 1353–1365.
- Valjent, E., Corvol, J.C., Pages, C., Besson, M.J., Maldonado, R.C., Caboche, J., 2000. Involvement of the extracellular signal-regulated kinase cascade for cocaine-rewarding properties. *J. Neurosci.* 20, 8701–8709.
- Valjent, E., Bertran-Gonzalez, J., Hervé, D., Fisone, G., Girault, J.-A., 2009. Looking BAC at striatal signaling: cell-specific analysis in new transgenic mice. *Trends Neurosci.* 32, 538–547.
- Westin, J.E., Vercammen, L., Strome, E.M., Konradi, C., Cenci, M.A., 2007. Spatiotemporal pattern of striatal ERK1/2 phosphorylation in a rat model of L-DOPA-induced dyskinesia and the role of dopamine D1 receptors. *Biol. Psychiatry* 62, 800–810.
- Winland, C.D., Welsh, N., Sepulveda-Rodriguez, A., Vicini, S., Maguire-Zeiss, K.A., 2017. Inflammation alters AMPA-stimulated calcium responses in dorsal striatal D2 but not D1 spiny projection neurons. *Eur. J. Neurosci.* 46, 2519–2533.
- Yang, L., Calingasan, N.Y., Lorenzo, B.J., Beal, M.F., 2008. Attenuation of MPTP neurotoxicity by rolipram, a specific inhibitor of phosphodiesterase IV. *Exp. Neurol.* 211, 311–314.
- Yapo, C., Nair, A.G., Clement, L., Castro, L.R., Hellgren Kotaleski, J., Vincent, P., 2017. Detection of phasic dopamine by D1 and D2 striatal medium spiny neurons. *J. Physiol. Lond.* 595, 7451–7475.
- Zhai, S., Ark, E.D., Parra-Bueno, P., Yasuda, R., 2013. Long-distance integration of nuclear ERK signaling triggered by activation of a few dendritic spines. *Science* 342, 1107–1111.
- Zhuang, X., Belluscio, L., Hen, R., 2000. G(olf)alpha mediates dopamine D1 receptor signaling. *J. Neurosci.* 20, RC91.